

Oil & Natural Gas Technology

DOE Award No.: DE-FC26-06NT43067

Coupled gas/water/sediment dynamics with rigid hydrate films (Task 7.1 Technical Report)

Mechanisms Leading to Co-Existence of Gas and Hydrate in Ocean Sediments

Submitted by:

The University of Texas at Austin
1 University Station C0300
Austin, TX 78712-0228

Prepared for:

United States Department of Energy
National Energy Technology Laboratory

October 30, 2009



Office of Fossil Energy

MECHANISMS LEADING TO CO-EXISTENCE OF GAS AND HYDRATE IN
OCEAN SEDIMENTS

CONTRACT NO. DE-FC26-06NT43067

Deliverable 7.1:

**Report on Task 7.0 "Coupled gas/water/sediment dynamics with hydrate
formation," Subtask 7.1 "Coupled dynamics with rigid hydrate films"**

October 30, 2009

Prepared by

Ruben Juanes

Department of Civil and Environmental Engineering
Massachusetts Institute of Technology
77 Massachusetts Avenue, Room 48-319
Cambridge, MA 02139
Phone: 617-253-7191, Fax: 617-258-8850
Email: juanes@mit.edu

and

Steven L. Bryant

Department of Petroleum and Geosystems Engineering
The University of Texas at Austin
1 University Station C0300
Austin, TX 78712-0228
Phone: (512) 471 3250
Email: steven_bryant@mail.utexas.edu

Prepared for

U.S. Department of Energy - NETL
3610 Collins Ferry Road
P.O. Box 880
Morgantown, WV 26508

Task 7.0 Coupled gas/water/sediment dynamics with hydrate formation

Ran Holtzman, Yao Peng, Steven Bryant and Ruben Juanes

OVERVIEW

Our premise is that hydrate forms from co-existing phases of gas and water in sediments. An important test of this premise is to assess hydrate growth at the grain scale, where the gas/water interface (GWI) is determined by capillarity. Another test of the premise is to assess the macroscopic consequences of the volume change associated with forming hydrate phase with components (CH_4 , H_2O) from the gas and aqueous phases. The volume change drives the pressure change and accompanying fluid displacement studied in the grain-scale model. At the macroscopic scale the pressure change caused by volume change drives grain movement, bulk phase fluid movement or both.

In Part 1 of this report we test our premise macroscopically, tabulating the fractional volume change as a function of temperature, pressure and salinity and identify a critical saturation of aqueous phase for hydrate conversion. We then consider implications of the limiting cases in which CH_4 and/or H_2O are available or not available for continued hydrate formation. In Part 2 we test our premise microscopically, applying models of capillarity-controlled gas/water displacement coupled to grain-scale mechanics developed previously in this project. We then develop plausible models of hydrate growth at the GWI and examine their implications for sediments of different grain size.

Part 1: Volume changes associated with equilibration of the CH_4 - H_2O -Methane Hydrate system

Simple Box Model

Figure 1 shows schematically a box of volume V . In this model, we only investigate the overall volume change due to hydrate formation. The location of hydrate formation within the volume (fluid/fluid or fluid/solid interface) is addressed in the microscale modeling section of this report.

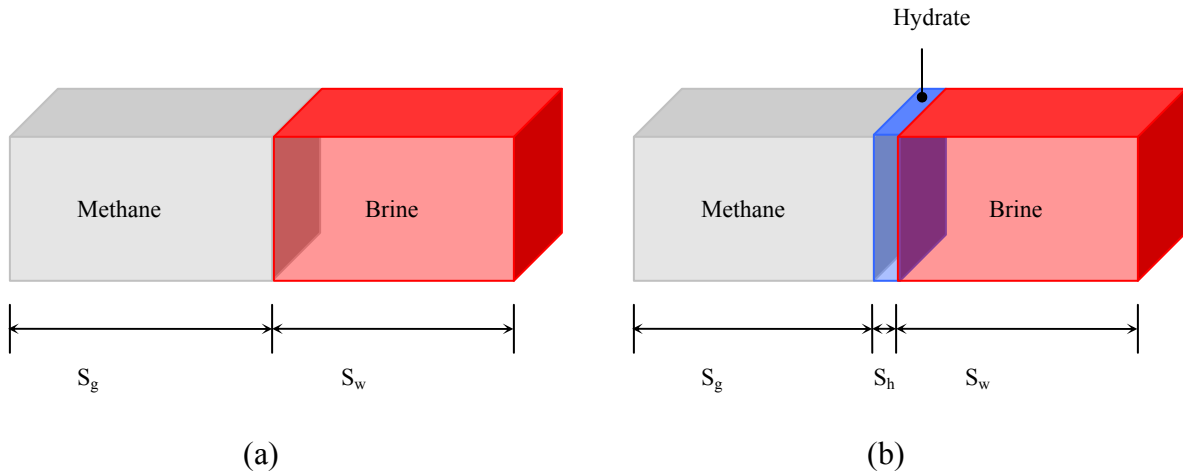


Figure 1. The box model to compute the volume change due to hydrate formation. (a) Initially no hydrate is present, the gas saturation is known, and $S_w = 1 - S_g$. (b) An increment of hydrate forms at the interface between gas and water phases.

The box can be imagined as a batch reactor in which we perform a classical "flash calculation" of the phases and compositions present at chemical equilibrium. The volume initially taken up by methane is denoted as $V S_g$, and by water as $V S_w$. The terms 'water' and 'brine' are used interchangeably in this report. No hydrate is initially present. If hydrate is thermodynamically stable at the temperature and pressure of the box, then we compute the amount that forms via a flash calculation. The resulting hydrate occupies a volume fraction denoted as S_h .

Due to the formation of hydrate, the volumes of brine and gas phases will change. In this study, we investigate the system volume change assuming the gas phase is pure methane and that gas phase density remains constant during hydrate formation. **That is, we assume T and P do not change during hydrate formation.** This assumption says in effect that the sediment grains will be rearranged and/or fluid phases will enter the box as needed to maintain pressure. At this point we do not concern ourselves with the reservoir dynamics or timescales to maintain the isothermal/isobaric state. The grain-scale dynamics for re-establishing pressure are described in the micro-scale modeling section of this report. The next two sections develop thermodynamic models needed for computing volume change in the box model.

Nomenclature

M_g	Molecular weight of methane (0.016 kg/mol)
M_w	Molecular weight of water (0.018 kg/mol)
N	Hydration number
P	Pressure (Pascal)
P_c	Pressure at the critical point (Pascal)
R	Ideal gas constant (8.314 J/(mol·K))
T	Temperature (K)
T_c	Temperature at the critical point (K)

V	System volume, or box volume (m ³)
V _g	Methane volume in the system (m ³)
V _w	Water volume in the system (m ³)
V _h	Hydrate volume in the system (m ³)
V _m	Molar volume, the volume of 1 mole of gas (m ³)
m _h	Mass of hydrate in the system (kg)
u	Mass of salt dissolved in brine (kg)
S _g	Initial gas phase saturation
S _w	Initial brine phase saturation
S _{wc}	Critical water saturation (maximum conversion of methane and water into hydrate is obtained when initial water saturation equals this value)
S _h	Hydrate saturation
x	Volume fraction of water that is converted into hydrate
Sal	Initial brine salinity (kg/kg)
MSal	Maximum brine salinity (kg/kg)
ρ _g	Methane density (kg/m ³)
ρ _{gc}	Critical methane density (kg/m ³)
ρ _w	Water density (kg/m ³)
ρ _h	Hydrate density (kg/m ³)
ω	acentric factor

Methane Density Variation under Different T and P

Methane density is computed by using the model proposed by Soave, Redlich and Kwong. The relationship between ρ_g , P and T are governed by the following system of equations:

$$P = \frac{RT}{V_m - b} - \frac{a\alpha}{V_m(V_m - b)} \quad (1)$$

$$a = \frac{0.42747R^2T_c^2}{P_c} \quad (2)$$

$$b = \frac{0.08664RT_c}{P_c} \quad (3)$$

$$\alpha = \left(1 + (0.48508 + 1.55171\omega - 0.15613\omega^2)(1 - T_r^{0.5})\right)^2 \quad (4)$$

$$T_r = \frac{T}{T_c} \quad (5)$$

$$\rho_g = \frac{M_g}{V_m} \quad (6)$$

T_c and P_c are the critical temperature and pressure, respectively. ω is the acentric factor. For methane, these values are: $T_c = 190$ K, $P_c = 4.64 \times 10^6$ Pa, $\omega = 0.011$. From the above system of equations, methane density is determined given the values of T and P .

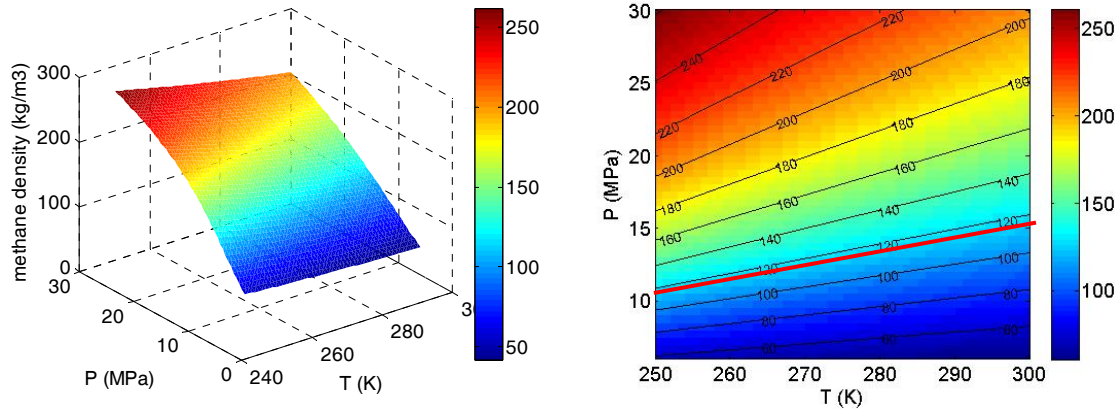


Figure 2. Methane density (kg/m^3) as a function of T and P (left is the surface plot and right is the contour plot). At lower pressure, methane density is a weak function of temperature, but a strong function of pressure. Methane density increases as increasing pressure or decreasing temperature. The red line on the contour plot is the equivalent CH_4 density in hydrate ($118 \text{ kg CH}_4/\text{m}^3$ hydrate).

The red line in the right panel of Figure 2 illustrates the methane molecule density in hydrate. This value is computed by using equation (30). If the gaseous methane density is greater than 118 kg/m^3 (region above the red line), the hydrate volume that is converted from methane will be greater than the volume of methane that is consumed, assuming that T and P are kept constant. On the other hand, below the red line where the gaseous methane density is smaller than 118 kg/m^3 , the opposite situation would happen. Thus system volume (methane+hydrate) change is inevitable as hydrate is generated, which leads to sediment compaction/fracture or fluid inflow/outflow in the Hydrate Stability Zone (HSZ).

Effect of Salinity on Hydrate Stability

Salt is an inhibitor for hydrate formation. At each combination of T and P , there is a maximum brine salinity, above which no hydrate can be generated and stably sustained. The maximum salinity, as well as T and P , defines the HSZ and affects the amount of hydrate in the sediments.

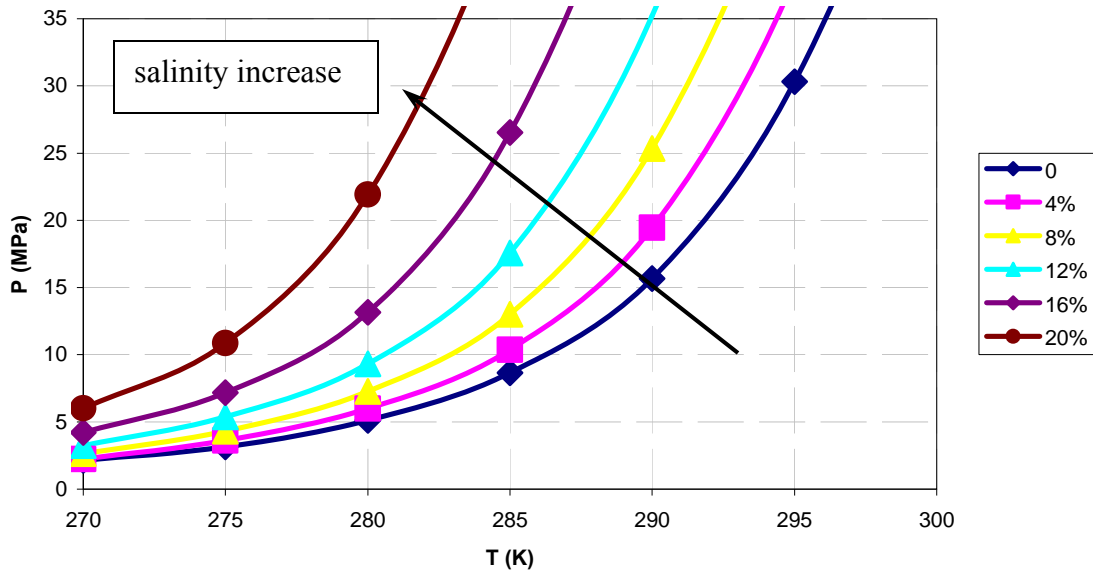


Figure 3. HSZ variation due to salinity of initially present brine. Contours shown for several values of wt % NaCl. Hydrate is stable above the curve, while unstable below it. With increasing salinity, HSZ retreats to a region of higher P and lower T , as shown by the arrow. The values (dots in the figure) are computed from: <http://www.geochem-model.org/models/ch4-sea/>

Figure 3 shows the salinity influence on HSZ. The curves are the phase boundaries (gas and water below, hydrate above) corresponding to various salinities. The increase of salinity moves the phase boundary to higher P and lower T , which shrinks HSZ. From salinity = 0 to 20%, a large region is lost from HSZ, showing a significant salinity effect.

Formulation

Limited Methane/Brine

In this scenario, the masses of CH_4 and of H_2O in the box are fixed at their initial values, that is, the box is closed after the initial saturations are set. This is the condition for the traditional batch equilibrium or flash calculation. Recall that T and P are assumed to remain constant when hydrate forms. The calculation uses brine density as $1,000 \text{ kg/m}^3$, and hydrate density as 914 kg/m^3 (Uchida et al., 1999; Hong et al., 2006). The hydration number N ($\text{CH}_4 \cdot N \text{H}_2\text{O}$) is set as 6.

With the changing of initial gas and water saturation, the amount of hydrate that can be generated varies accordingly. We define the **critical water saturation** (S_{wc}) as value at which both gas and water phases are completely, stoichiometrically converted into hydrate, if it is fresh water. If the aqueous phase is brine, the critical water saturation is the value at which the gas phase can be converted completely, and brine phase can be converted maximally (that is, the salinity of the remaining brine is the maximum salinity for stable hydrate phase at that T and P). When $S_w < S_{wc}$, methane is excessive and gas phase remains after all the water is converted; when $S_w > S_{wc}$, water is excessive and the brine phase remains after all the CH_4 is converted. We first develop the formulation to predict S_{wc} , and then discuss the situations of excessive methane and water, respectively.

In order to generate a quantity m_h of hydrate, we need the following volume of gas and fresh water:

$$V_g = \frac{m_h \frac{M_g}{M_g + NM_w}}{\rho_g} \quad (7)$$

$$V_w = \frac{m_h \frac{NM_w}{M_g + NM_w}}{\rho_w} \quad (8)$$

For maximum conversion of methane, i.e. complete conversion of the methane in the gas phase to hydrate, we require that

$$V_g = VS_g \quad (9)$$

and for a maximum conversion of water,

$$V_w = VS_w x \quad (10)$$

The coefficient x is unity if the water is fresh. Unlike the gas phase, the water phase cannot be totally converted into hydrate because of the salt dissolved in it. We account for this with coefficient x , with $x = 1$ for pure water and $x < 1$ for brine.

By the definition of initial salinity Sal , we have

$$\frac{u}{V_w \rho_w + u} = Sal \quad (11)$$

As hydrate forms in this scenario, it rejects salinity ions, forcing them to remain in the water phase. Thus the salinity in the remaining brine will increase as hydrate forms. When the initial salinity increases to the maximum salinity for hydrate stability, none of the water remaining in the box can be used to generate hydrate (in this closed-box scenario). The maximum salinity $MSal$ is related to x , the fractional conversion of water to hydrate, by

$$\frac{u}{V_w \rho_w (1-x) + u} = MSal \quad (12)$$

The maximum salinity is a function of T and P , as shown in Figure 3.

Combining equation (11) and (12), we have

$$x = \left(1 - \frac{Sal}{MSal}\right) \left(1 + \frac{u}{V_w \rho_w}\right) \quad (13)$$

Also from equation (11), it is easy to get

$$\frac{u}{V_w \rho_w} = \frac{Sal}{1 - Sal} \quad (14)$$

Equation (13) and (14) yield

$$x = \left(1 - \frac{Sal}{MSal}\right) \frac{1}{1 - Sal} \quad (15)$$

We can combine equation (7), (8), (9), (10), (15) to get the critical water saturation, given the initial salinity and the temperature and pressure of the sediment:

$$S_{wc} = 1 - \frac{1}{1 + \frac{\rho_g}{\rho_w} \frac{NM_w}{M_g} \frac{1 - Sal}{\left(1 - \frac{Sal}{MSal}\right)}} \quad (16)$$

When initial salinity $Sal = 0$, equation (16) is reduced to

$$S_{wc} = 1 - \frac{1}{1 + \frac{\rho_g}{\rho_w} \frac{NM_w}{M_g}} \quad (17)$$

The hydrate saturation, after the maximum conversion of gas and water under the critical water saturation (S_{wc}), is:

$$S_h = xS_{wc} \frac{\rho_w}{\rho_h} \frac{NM_w + M_g}{NM_w} \quad (18)$$

The aqueous phase saturation after maximum conversion is zero if the initial salinity is zero; otherwise it is $(1-x)S_{wc}$.

Equation (18) shows hydrate saturation resulting when $S_{wl} = S_{wc}$ is a direct function only of initial salinity, as the other parameters are all constant at a given T and P . The volume reduction when hydrate formation is complete is the original system volume V minus the volume of hydrate VS_h formed (equation (18)) and volume of brine remaining $(1-x)VS_{wc}$. The relative volume reduction is thus

$$\frac{dV}{V} = 1 - \left(xS_{wc} \frac{\rho_w}{\rho_h} \frac{NM_w + M_g}{NM_w} + (1-x)S_{wc} \right) \quad (19)$$

$S_w > S_{wc}$

When $S_w > S_{wc}$, water is excessive. Methane is the limiting reactant in the hydrate formation, and all the CH_4 in the initial gas saturation is converted to hydrate. In this case the volume change of the system (gas+water+hydrate) can be computed from initial gas saturation S_g .

Since gas is totally converted into hydrate, with V_g amount of gas ($V_g = VS_g$), we can generate the following V_h amount of hydrate.

$$V_h = \frac{VS_g \rho_g}{\rho_H} \frac{M_g + NM_w}{M_g} \quad (20)$$

and also require the following amount of water.

$$V_w = \frac{VS_g \rho_g}{\rho_w} \frac{NM_w}{M_g} \quad (21)$$

The volume change of the system is defined as

$$dV = dV_h + dV_w + dV_g \quad (22)$$

Because hydrate is generated, and water and gas are consumed, dV_h is positive and dV_w and dV_g are negative. The volume change of the system as fraction of the initial volume is derived from equation (20) and (21).

$$\frac{dV}{V} = S_g \left(\frac{\rho_g}{\rho_h} \frac{M_g + NM_w}{M_g} - \left(1 + \frac{\rho_g}{\rho_w} \frac{NM_w}{M_g} \right) \right) \quad (23)$$

where dV/V is the volume change as a fraction of the initial volume. It clearly indicates that gas saturation S_g determines the final volume change. The density of the gas phase also has a first-order influence on dV/V .

$S_w < S_{wc}$

When $S_w < S_{wc}$, methane is excessive. The conversion to hydrate will be limited by the availability of water and/or the salinity. The volume change of the system is thus derived in terms of the water saturation.

Because of initial salinity effect, water cannot be completely converted into hydrate. Hydrate can keep growing until the initial salinity reaches the maximum salinity at the given T and P . The volume fraction of water that can be converted into hydrate is determined by equation (15). The converted water volume is

$$V_w = xVS_w \quad (24)$$

where x is a function of initial salinity, T and P ; x is computed from equation (15). V_w of water yield a volume V_h of hydrate according to

$$V_h = \frac{xVS_w \rho_w}{\rho_h} \frac{M_g + NM_w}{NM_w} \quad (25)$$

and the required gas V_g can be easily computed from the above equation

$$V_g = \frac{xVS_w \rho_w}{\rho_g} \frac{M_g}{NM_w} \quad (26)$$

The volume change, defined by equation (22), as a fraction of the initial volume is computed as

$$\frac{dV}{V} = xS_w \left(\frac{\rho_w}{\rho_h} \frac{M_g + NM_w}{NM_w} - \left(1 + \frac{\rho_w}{\rho_g} \frac{M_g}{NM_w} \right) \right) \quad (27)$$

Summary

We have developed the formulation to determine the volume change when initial saturations of gas and brine phases are specified and neither CH_4 nor H_2O enter the volume. We find the critical water saturation S_{wc} , equation (16) and (17), at which all the gas phase saturation and the maximum possible amount of the water phase are converted to hydrate. The volume change for cases of $S_w > S_{wc}$, equation (23), and $S_w < S_{wc}$, equation (27), are also derived.

Since at $S_w = S_{wc}$, all methane in the system is converted into hydrate, and the maximum water is also converted, the volume change resulting from this initial condition is the largest possible. That is, for any $S_w \neq S_{wc}$, the magnitude of the volume change is smaller than at S_{wc} . Both cases ($S_w = S_{wc}$ and $S_w \neq S_{wc}$) are discussed in the report.

Limited Methane, Unlimited Brine

We now consider volume changes when the system is open to influx of brine, but the mass of methane in the box remains fixed at its initial value. The concept of critical water saturation is no longer relevant in this situation. We assume that brine enters the box so as to keep the brine saturation constant. In effect, then, the hydrate occupies space originally filled with gas phase. This can be regarded as the macroscopic consequence of hydrate film rupture followed by imbibition, discussed in the microscale modeling section.

As in the scenario of limited methane/limited brine discussed previously, we assume that the temperature and pressure in the box do not change. Finally we assume that the salinity remains constant. This means that the salt buildup associated with hydrate formation diffuses away instantaneously.

The system volume change is only related to the volume of methane consumed and the volume of hydrate generated, since the volume of brine is considered constant.

For V_g of methane consumed, we have V_h of hydrate:

$$V_h = VS_g \frac{\rho_g}{\rho_h} \frac{M_g + NM_w}{M_g} \quad (28)$$

Therefore, since all hydrate grows into the volume occupied by methane, the system volume change is:

$$\frac{dV}{V} = S_g \left(\frac{\rho_g}{\rho_h} \frac{M_g + NM_w}{M_g} - 1 \right) \quad (29)$$

Equation (29) indicates that there is a value of gas phase density at which the system volume would be unchanged after hydrate formation, i.e. $dV = 0$. This critical methane density should satisfy the following equation.

$$\rho_{gc} = \rho_h \frac{M_g}{M_g + NM_w} \quad (30)$$

The T and P of the system determine the gas phase density. When ρ_g is greater than critical gas density, the system volume will **increase** due to the hydrate formation. On the other hand, system volume will **decrease** if ρ_g is less than the critical gas saturation. Since the right hand side of equation (30) consists of constants, ρ_{gc} is easily calculated.

$$\rho_{gc} = 914 \frac{16}{16 + 6 \times 18} = 118 \text{ kg} / \text{m}^3 \quad (31)$$

At the T and P characteristic of the hydrate stability zone, gas density is usually less than $100 \text{ kg}/\text{m}^3$; see Figure 2. This means the system volume will usually decrease in the present scenario (limited methane, unlimited brine). The situation that system volume increases is theoretically possible, for example in water depths greater than 1500 m with a seafloor temperature of 277 K.

Results and Discussion

Limited Methane/Brine

Critical Water Saturation (S_{wc})

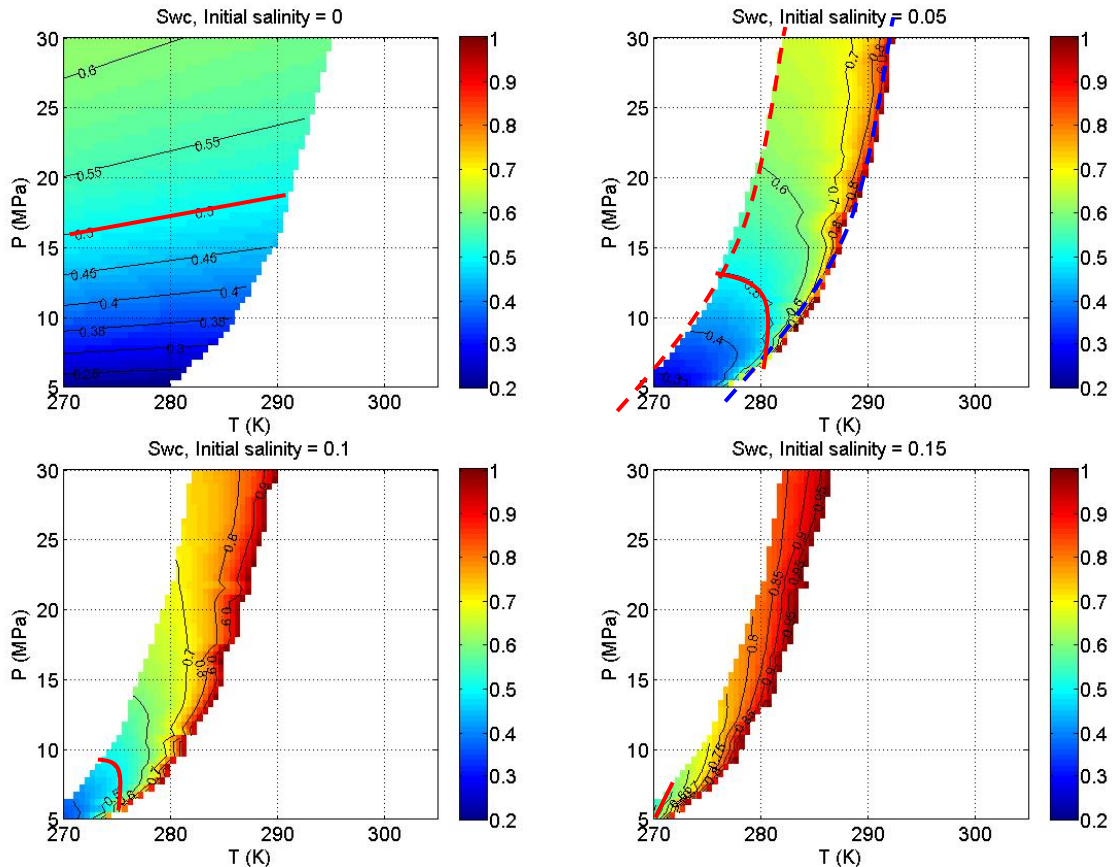


Figure 4. Critical water saturation as a function of T and P for four different initial salinities. The blank region on the right hand side of each plot (boundary indicated by dashed blue curve in top right panel) exists because hydrate is not stable in this region. The blank region on the left hand side of each plot (boundary indicated by dashed red curve in top right panel) is because our equation of state does not extend beyond salinity of 20%.

When the initial water saturation in a closed volume is equal to the critical water saturation, then all the initial gas saturation and the maximum possible amount of the water saturation will be converted to hydrate. When $Sal = 0$ (Figure 4, top left), the critical water saturation is a strong function of pressure (large variation with changing pressure), but a weak function of temperature (small variation with changing pressure). From equation (17), variation of S_{wc} is driven by variation of ρ_g , as the other parameters are constants or, in the case of water density, nearly constant. Figure 2 shows ρ_g depends strongly on pressure but weakly on temperature. This causes the dependence of S_{wc} on T and P shown in Figure 4.

At zero initial salinity, S_{wc} increases as the system pressure increases. Methane has a low density when pressure is low. It requires less volume of water to totally convert water and

methane into hydrate, which means the volume fraction of water initially present in the system must be smaller in order to achieve complete conversion of both phases to hydrate. When methane density increases due to high pressure, more water is needed to totally convert the same volume of gas, which boosts the required initial volume fraction of water in the system.

In other cases when $Sal \neq 0$ (Figure 4, top right and bottom panels), S_{wc} behaves differently. S_{wc} increases with temperature as well as pressure. The maximum S_{wc} is on the right boundary of the region. This is because here the initial salinity of water is close to the maximum salinity for hydrate stability under that T and P . Only a small amount of water can be converted to hydrate as the initial salinity will increase immediately to the maximum salinity. Consequently only a small amount of methane can be converted.

S_{wc} has a great variation at different T and P , which often ranges from 30% to 90%. This also leads to the large variation in the amount of hydrate generated. As discussed below, hydrate formation generally reduces the volume occupied by the gas, aqueous and hydrate phases. The manner in which this volume is filled is of great interest, because it changes the pore pressure in the sediments, which then can cause fracturing, compaction, or fluid displacement. Any of these events can create new gas/water interfaces, leading to a feedback loop that will influence the growth habit of hydrates.

Hydrate Saturation

The hydrate saturation obtained when the initial aqueous phase saturation equals the critical saturation is shown in Figure 5. The calculation gives the maximum hydrate saturation that could possibly be generated from limited gas and water if T and P remain constant. For example, at $P = 10$ MPa and $T = 280$ K, the maximum hydrate saturation would be 37%, if the initial salinity were 5 wt%.

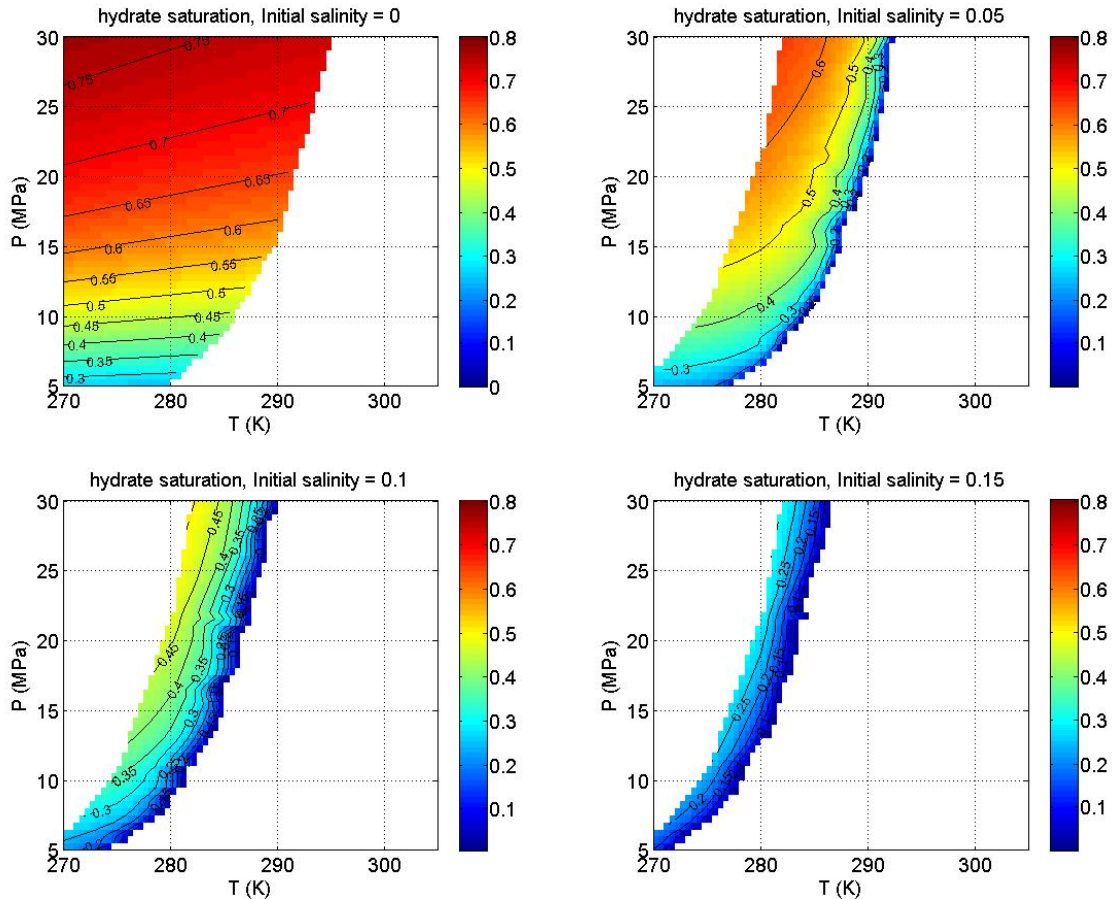


Figure 5. The hydrate saturation resulting from conversion of all initial gas phase at different Sal , T and P , when initial aqueous phase saturation is equal to critical saturation of Figure 4. The reason for the blank regions is the same as in Figure 4.

At initial salinity = 0, Figure 5 shows similar behavior as Figure 4. At low pressure, the mass of methane initially present is smaller, so that the final hydrate saturation is also relatively small. When initial salinity $\neq 0$, the hydrate saturation increases from the right to the left boundary. On the right boundary, not much hydrate can be generated because the initial water salinity is already close to the maximum salinity.

Initial water salinity plays a significant role in hydrate saturation. For example at $T = 280$ K and $P = 15$ MPa, S_h reaches 50% at initial salinity equal to 5%, while S_h is only 15% at initial salinity equal to 15%. This has implications for the possible hydrate saturation in arctic or permafrost regions, where brine salinity may vary substantially. At the same T

and P , lower initial salinity always leads to higher hydrate saturation. This is because much more fresh water can be provided to generate hydrate when initial salinity is lower.

In most cases the salinity in sea water is lower than 3%. With this salinity, the maximum hydrate saturation is plotted in the Figure 6. For the conditions at Hydrate Ridge, S_h formed in this scenario ranges from 30% to 50%, depending on T and P . In Blake Ridge, due to its high T and P , this scenario leads to larger S_h (around 60%). For Mt. Elbert, the maximum hydrate saturation is around 30%, based on the limited methane/brine scenario. However, such prediction underestimates the field observation, which shows a maximum of 70% S_h . Therefore, this scenario, limited methane/brine, is not applicable to the case of Mt. Elbert.

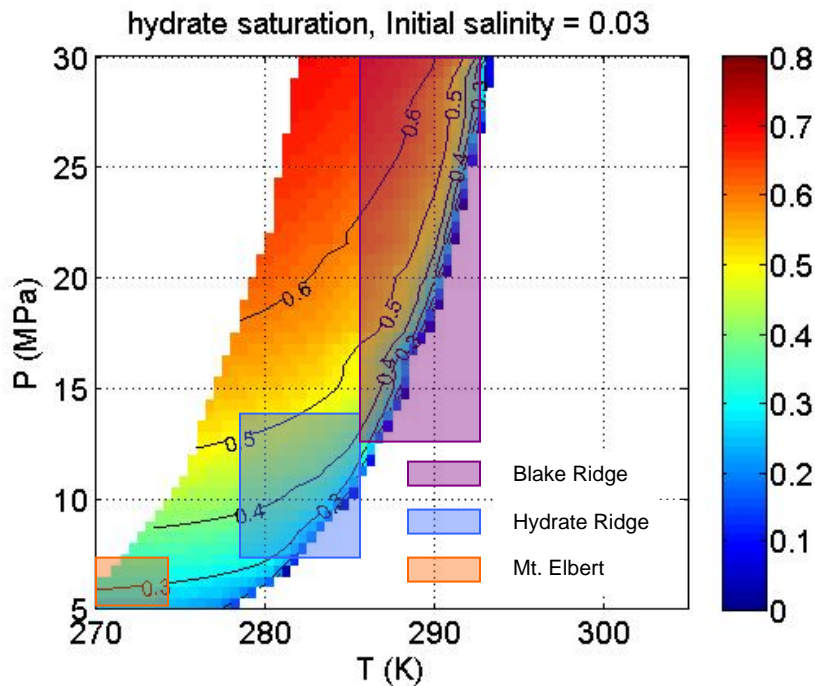


Figure 6. Hydrate saturation at sea water salinity (3%), at different T and P . The hydrate saturation is computed at S_{wc} , which results in the maximum hydrate saturation in the system. It also shows the $T - P$ range of different hydrate reservoirs. The region beyond the right boundary should be neglected, as hydrate is not stable there.

Remaining Brine Saturation (S_{br})

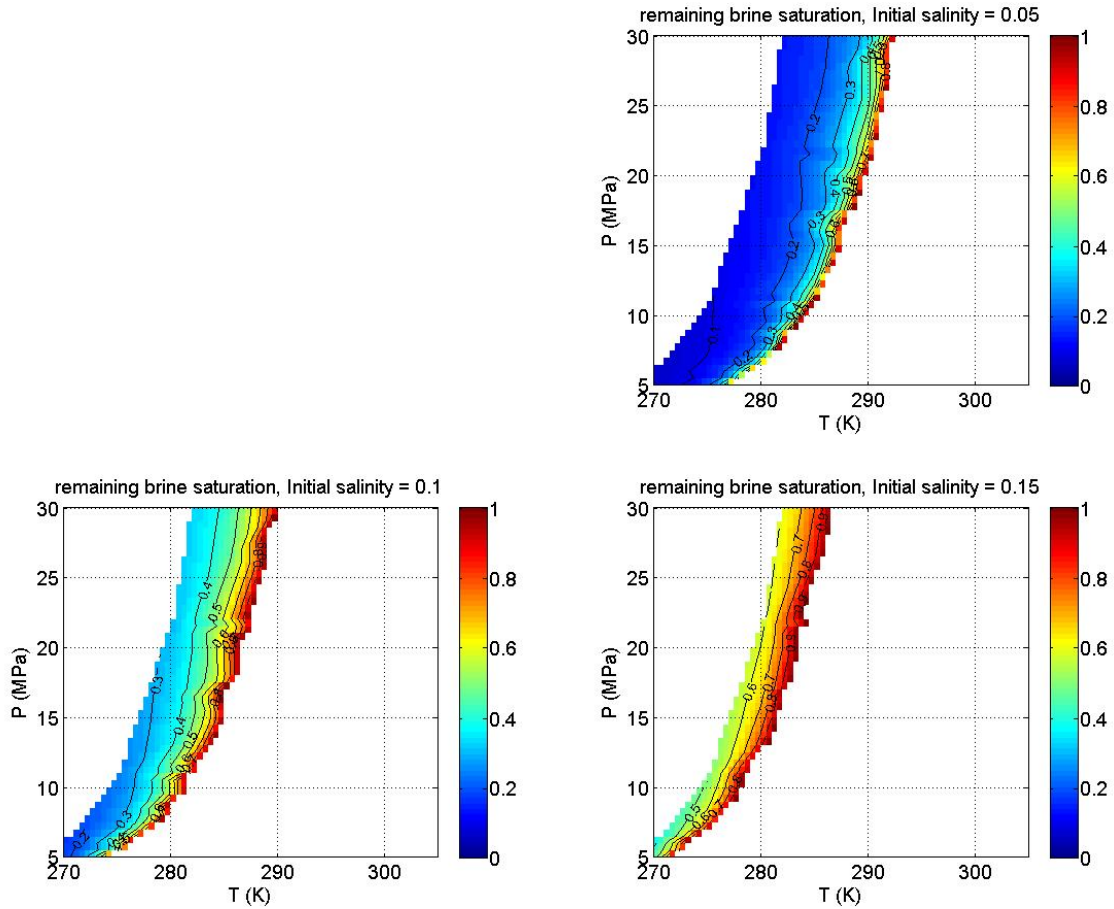


Figure 7. Remaining brine saturation after hydrate conversion is complete.

The remaining brine saturation (S_{br}) is calculated after hydrate conversion is complete. When initial salinity = 0, no water remains, so that S_{br} is zero at all T and P . As salinity increases, S_{br} at a specific T and P increases substantially, due to the inhibitive effect of salinity to hydrate formation. At a given salinity, S_{br} increases towards the right boundary, where the initial salinity is close to the maximum salinity.

System Volume Reduction at $S_w = S_{wc}$

Because methane is totally consumed under the critical water saturation, only two phases – hydrate and brine – remain after the maximum conversion.

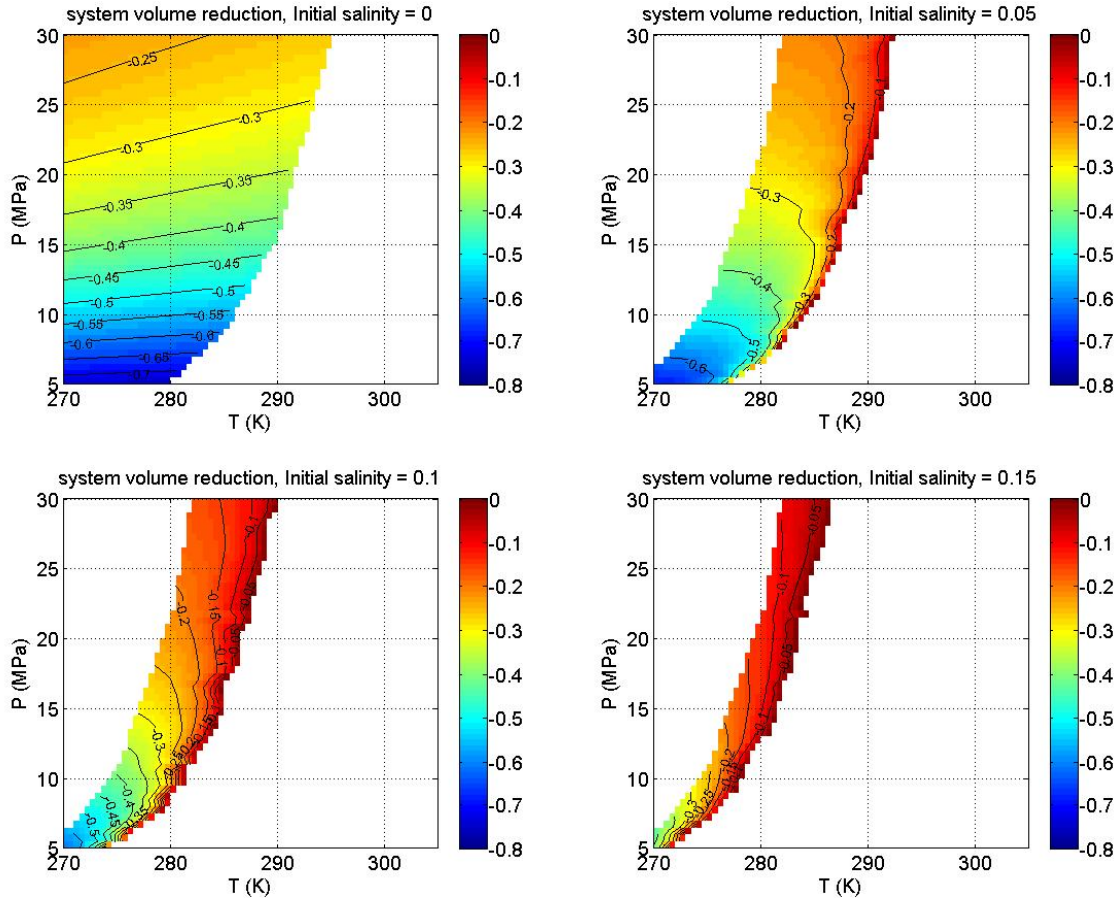


Figure 8. System volume reduction at S_{wc} . The color bar has the negative sign. The reason for the blank regions is the same as in Figure 4.

For all cases shown in Figure 8, the system volume decreases when hydrate forms from gas and water phases. The maximum reduction ($> 70\%$) happens at low pressure when $Sal = 0$. The minimum reduction (almost 0) is when the initial salinity is close to the maximum salinity, which means almost no hydrate is generated. At the low salinity condition ($Sal = 5\%$), large volume reduction (40% to 50%) can be observed at low P and T . If this occurs in shallow oceanic sediments, such large vacancy will lead to strong competition between sediment compaction and fluid displacement. If fluid displacement occurs, the volume change is smaller and is discussed in the next section.

The implications of the reduction of volume occupied by phases are significant in sediments. Because hydrate and water are not compressible, the final volume of hydrate and brine decides the sediment behavior. If the final volume of hydrate and water is smaller than the initial system volume (gas + water phases), and if neither gas nor aqueous phases can enter the system, then sediment compaction must occur.

System Volume Reduction at $S_w \neq S_{wc}$

Given the importance of the sign of the volume change (negative means volume reduction, requiring sediment compaction if fluids cannot enter; positive means volume increase, resulting in fracturing if fluids cannot escape), it is useful to examine the

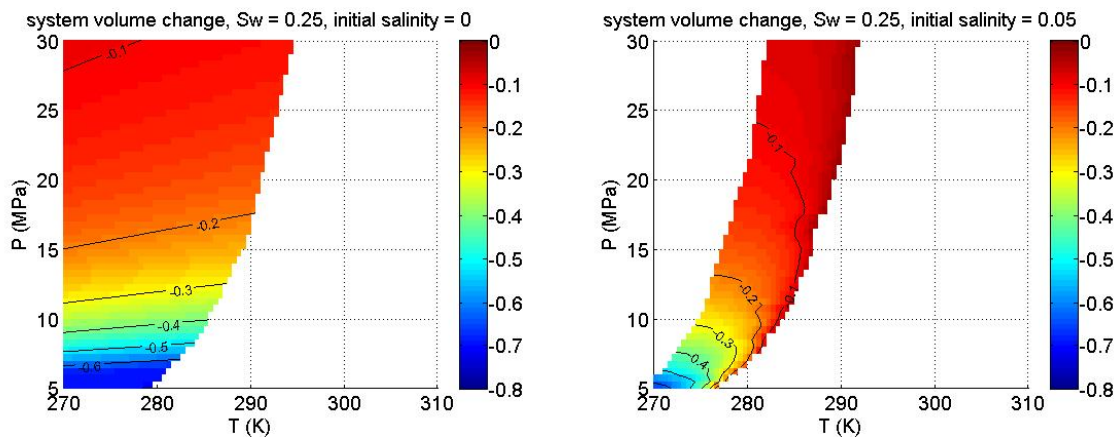
behavior for a range of initial conditions such that S_w differs from the critical value S_{wc} . Figure 10, 10, and 11 show the results for initial S_w of 0.25, 0.5 and 0.75, respectively. Depending on the relative amounts of methane and brine, the system volume reduction can be determined either by using equation (23) or (27).

At $S_w = 0.25$, the system volume decreases at all salinities (Figure 9). From Figure 4 we see that $S_{wc} = 0.25$ is very close to the left boundaries for all initial salinities. Therefore, $S_w = 0.25$ is smaller than S_{wc} in most part of the P - T domain. The system volume reduction at $S_w = 0.25$, at a specific T and P , is always less than the corresponding point when $S_w = S_{wc}$ (Figure 8).

At $S_w = 0.5$, we also observe system volume reduction at all salinities (Figure 10). In Figure 4, we labeled $S_{wc} = 0.5$ with the red curve. Comparing Figure 8 and Figure 10 shows that the volume reduction always has smaller magnitude when S_w differs from S_{wc} . Thus calculations of the effect of the volume change made at S_{wc} provide an upper bound on the actual behavior.

At $S_w = 0.75$, although we also observe volume reduction at all salinities, the magnitude is much smaller compared with $S_w = 0.25$ or 0.5. However, similar to $S_w = 0.25$ or 0.5, the largest volume reduction occurs at low P and T , where methane density is relatively low.

The situation $S_w = 0.25$ is representative of a drainage endpoint, where wetting phase has been largely displaced by invading gas phase, leaving some remaining wetting phase trapped in pores or corners. $S_w = 0.5$ can be considered as the mid point of drainage/imbibition, when wetting and nonwetting phases are all connected with the bulk. $S_w = 0.75$ resembles the case of imbibition endpoint, where gas phase has been displaced by wetting phase down to its residual saturation; in this case S_{gr} would be 0.25. As S_w increases from 0.25 to 0.75, the amount of volume change is smaller. Thus converting brine and methane at drainage endpoint will cause a larger volume reduction than at intermediate saturations, and converting residual gas to hydrate will induce the smallest volume change. Even at residual saturations, however, the volume reduction could be 20% under typical ocean sediment conditions.



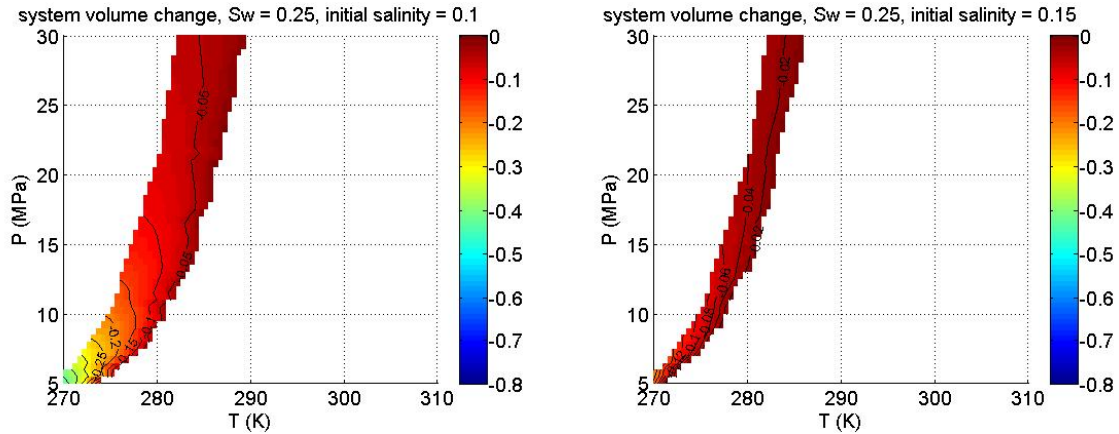


Figure 9. System volume reduction when $S_w = 0.25$. The color bar has negative signs. The calculation assumes the maximum conversion into hydrate, assuming that no additional CH_4 nor H_2O enters the volume.

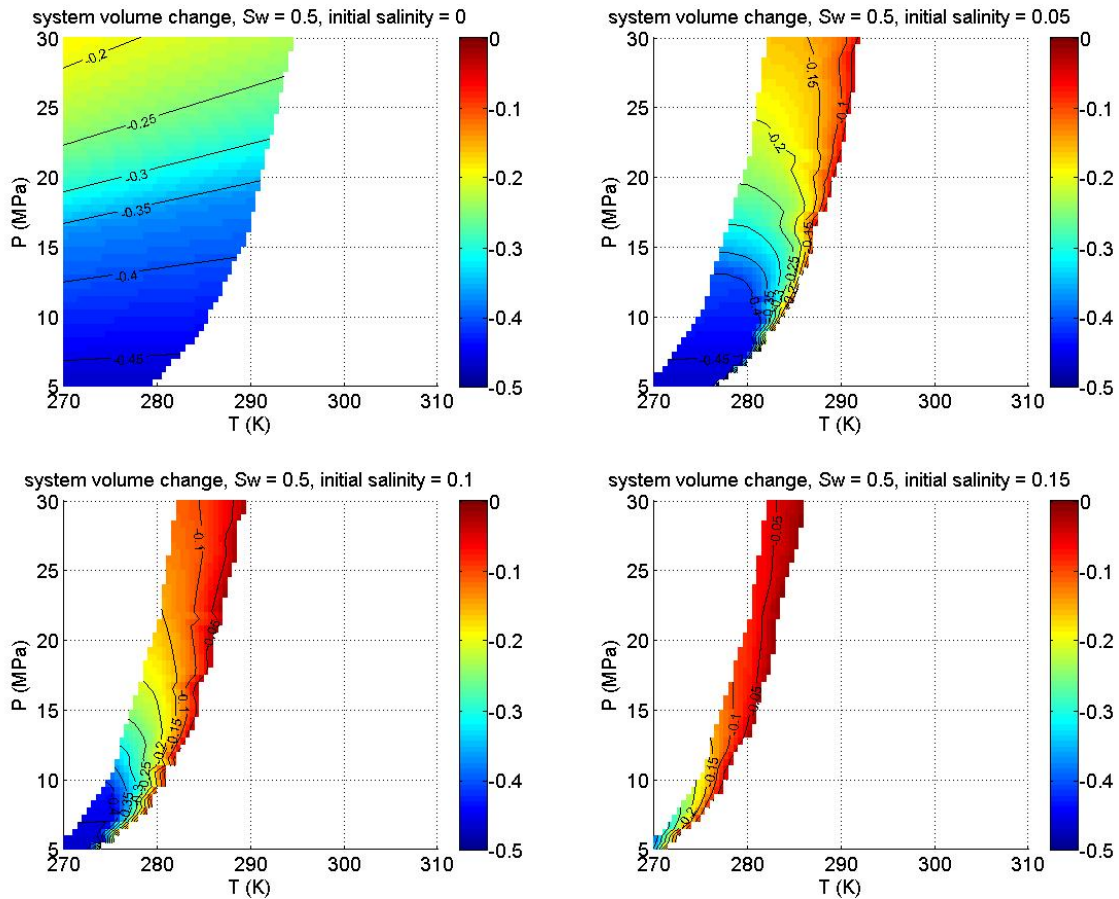


Figure 10. System volume reduction when $S_w = 0.5$. The color bar has negative signs. The calculation assumes the maximum conversion into hydrate, assuming that no additional CH_4 nor H_2O enters the volume.

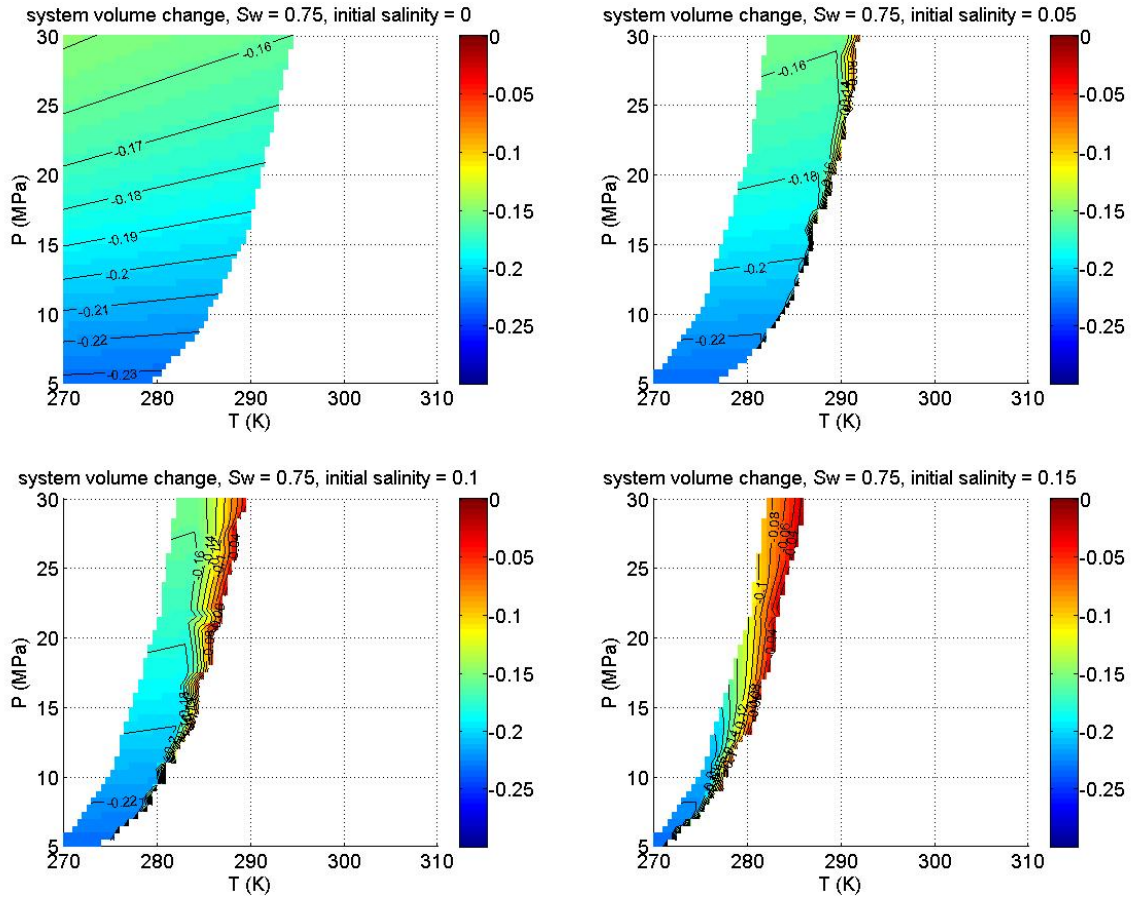


Figure 11. System volume reduction when $S_w = 0.75$. The color bar has negative signs. The calculation assumes the maximum conversion into hydrate, assuming that no additional CH_4 nor H_2O enters the volume.

Limited Methane, Unlimited Brine

In this section, we consider a scenario that methane is limited, but brine is unlimited. The hydrate generation is considered to be much slower than the salt diffusion in the brine. Therefore, the salt ions concentrated as water is converted to hydrate will not accumulate and inhibit the hydrate generation. Salinity is not a determinant in the calculation.

Critical Water Saturation (S_{wc})

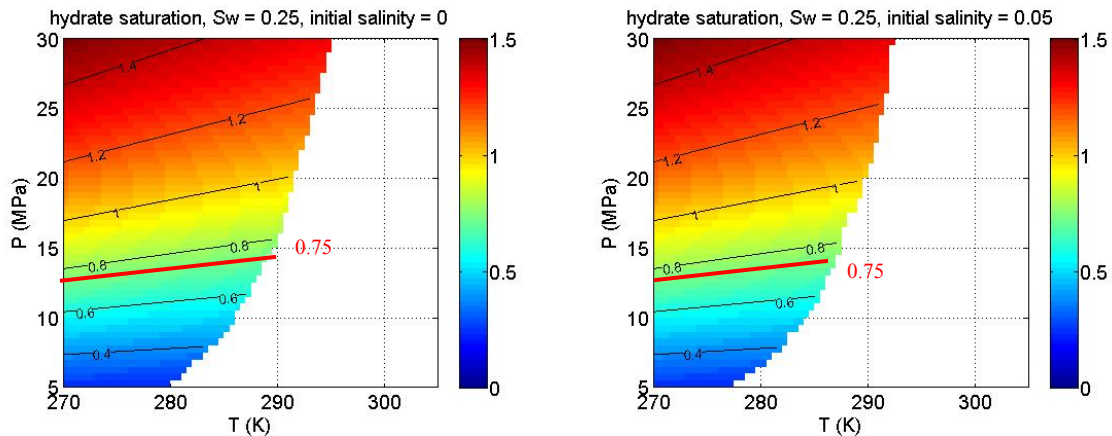
Recall that S_{wc} is not relevant because brine is unlimited. We assume instead that the initial S_w remains constant as hydrate forms.

Hydrate Saturation

Because of the unlimited brine, the hydrate saturation is determined by the amount of methane in the system.

Figure 12 shows the hydrate saturation computed from equation (28) at different salinities for initial $S_w = 0.25$. Because S_w is fixed as 0.25, S_g is 0.75, and this saturation determines the volume that will be occupied by hydrate. We labeled the contour of $S_h = 0.75$ as the red curve. When S_h is greater than 0.75, the volume occupied by hydrate will be greater than the volume originally occupied by methane, which leads to the system volume increment. However below the red curve, hydrate volume is smaller than the methane volume, so that the system volume will decrease as methane is converted into hydrate. Hydrate saturations that exceed unity are obviously nonphysical but are included for generality. The meaning of this region of the plot is the same as for $S_h > 0.75$, namely that the system pore volume would have to increase to accommodate the hydrate.

The effect of salinity is only to determine the right boundary of the region, that is, the boundary beyond which hydrate is not stable. Since we assume salinity does not accumulate in the brine as hydrate is formed, hydrate saturation does not vary with proximity to the stability boundary.



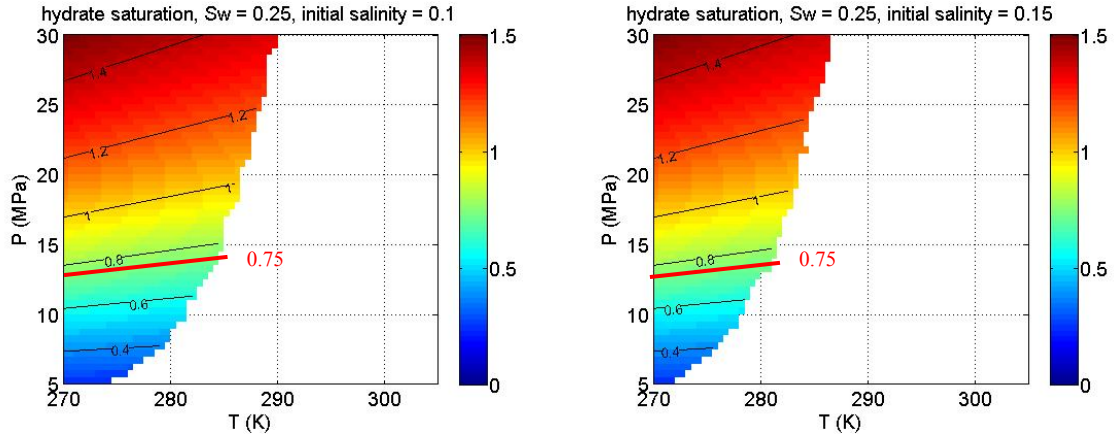
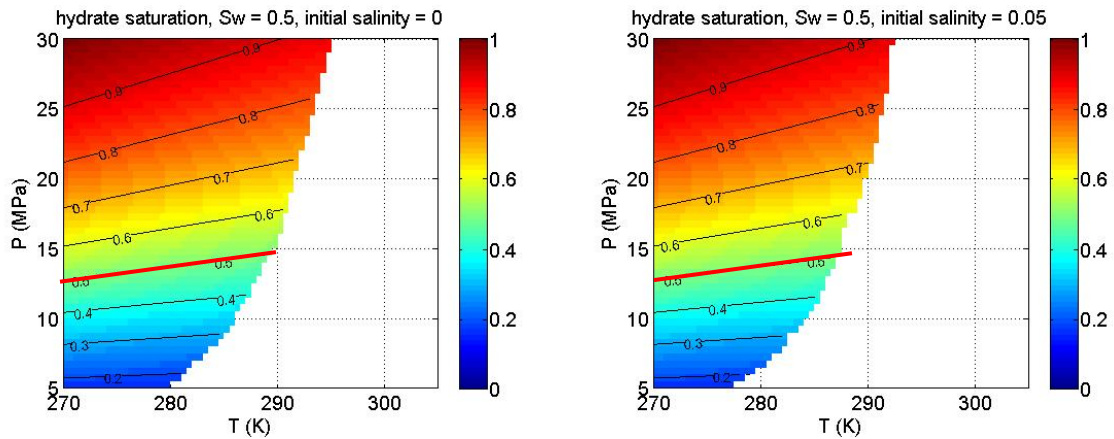


Figure 12. Hydrate saturation resulting from $S_w = 0.25$, at four salinities. Since water is unlimited, water saturation is constant. There is no supply of methane from outside the system.

Figure 13 shows hydrate saturation resulting from initial $S_w = 0.5$ at four different salinities. The initial methane saturation S_g is $1 - S_w = 0.5$, which is labeled as the red curve. When hydrate saturation is greater than 0.5, it means the hydrate volume is greater than the initial methane volume. Consequently the system volume increases. When hydrate saturation is smaller than 0.5, the opposite situation holds, that is, the system volume decreases.

The similar analysis can also be applied to explain Figure 14, where the initial S_w is 0.75. Here, the contour of $S_w = 0.25$ becomes the boundary for system volume increment or reduction: above that curve, system volume will increase, and below it system volume will decrease.

Figure 12, Figure 13 and Figure 14 all show the identical location the red curve. This location corresponds to the constant methane density of 118 kg/m^3 (the red curve on the right panel of Figure 2). As discussed, above this curve the methane density is greater than the methane molecule density in hydrate; therefore hydrate volume that is generated will be greater than the methane volume that is consumed. On the other hand, below the curve the methane density is smaller than the methane molecule density in hydrate, so that hydrate volume will be smaller than the methane volume.



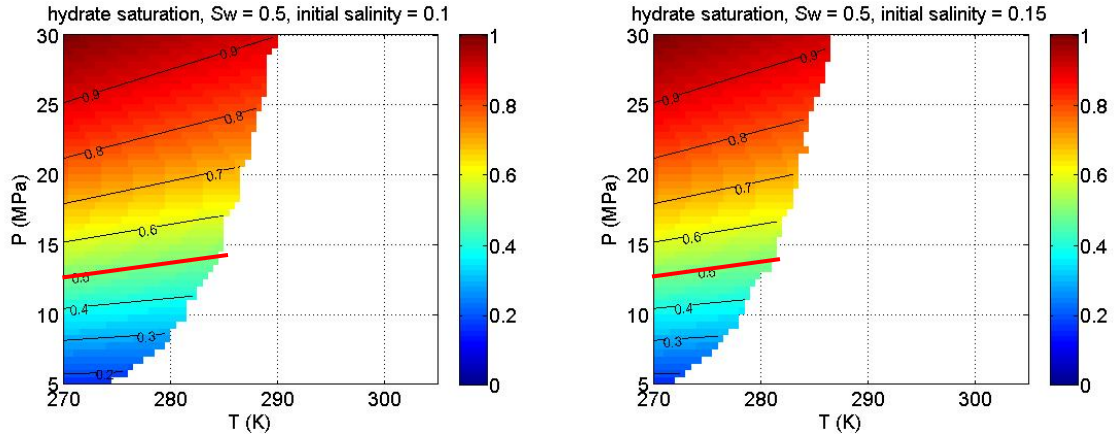


Figure 13. Hydrate saturation resulting from $S_w = 0.5$, at four salinities. Since water is unlimited, water saturation is constant. There is no supply of methane from outside the system.

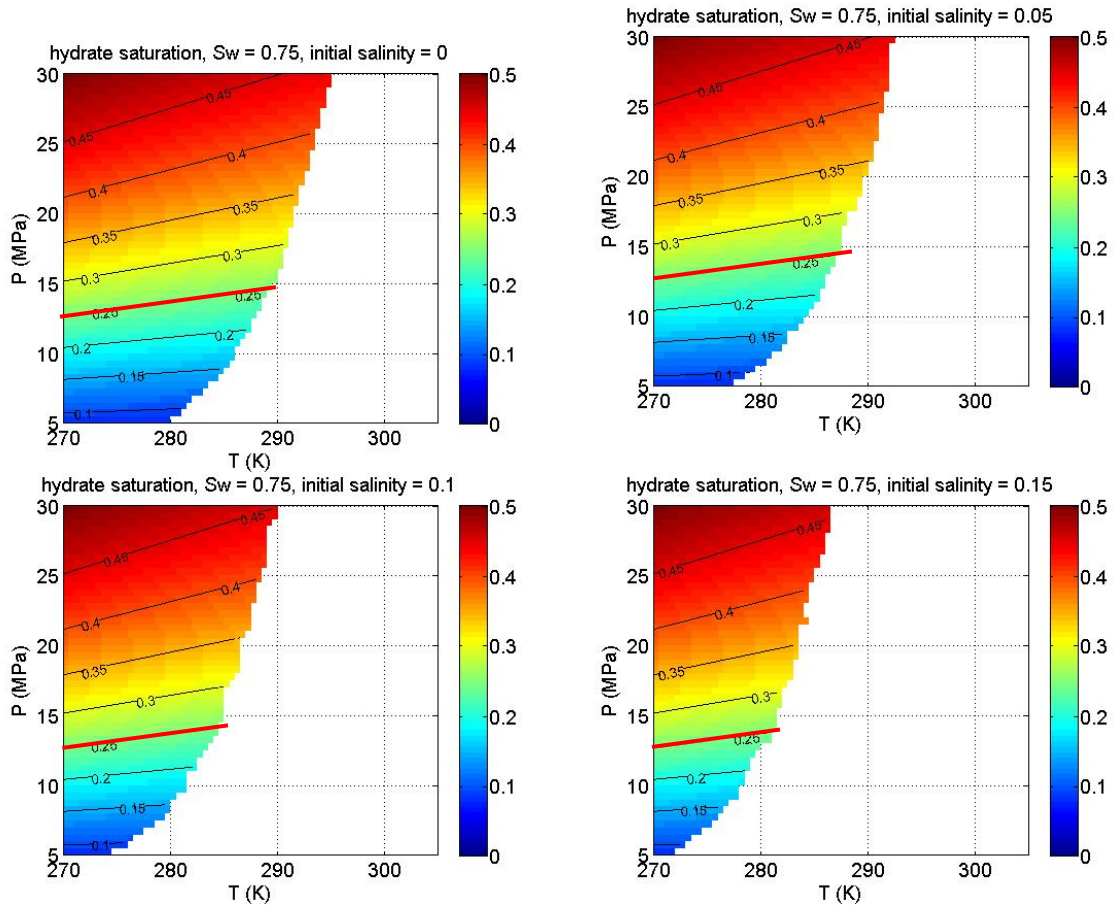


Figure 14. Hydrate saturation resulting from $S_w = 0.75$, at four salinities. Since water is unlimited, water saturation is constant. There is no supply of methane from outside the system.

System Volume Change

Because S_{wc} is not defined in this scenario, system volume reduction at $S_w = S_{wc}$ and $S_w \neq S_{wc}$ is not relevant. Instead we analyze the system volume change based on the initial gas saturation from equation (29).

Figure 15 shows the system volume change with limited methane and unlimited brine. When the contour value is 0, the volume of methane converted is equal to the volume of hydrate formed, and the system volume remains unchanged. Above this contour, the system volume increases as the methane density is greater than the critical density; while below the contour the system volume will decrease.

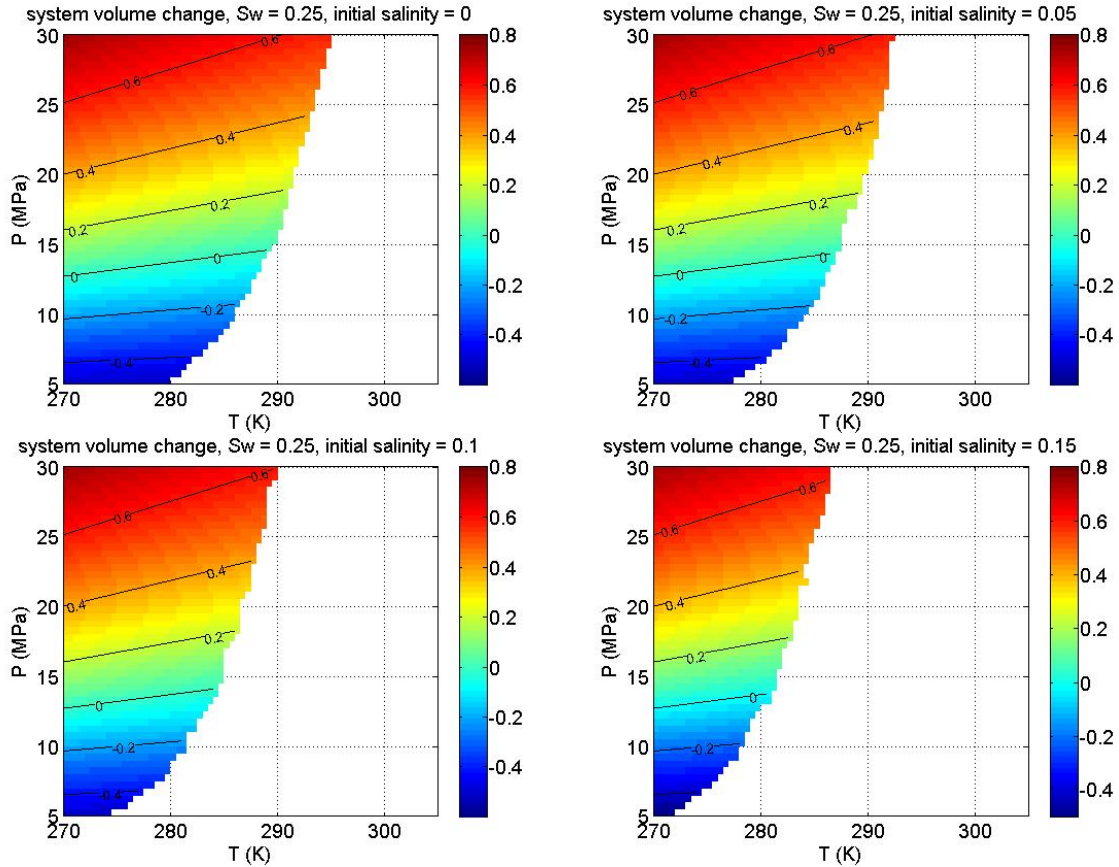


Figure 15. System volume change at $S_w = 0.25$, at four salinities. Since water is unlimited, water saturation is constant. There is no supply of methane from outside the system.

Figure 16 shows the system volume change at $S_w = 0.5$. Contour = 0 is at the same location as in Figure 15, where the methane density is equal to the critical methane density. The volume change can also be positive or negative, depending on the region is above or below contour = 0. Similar behavior can also be observed in Figure 17, where $S_w = 0.75$.

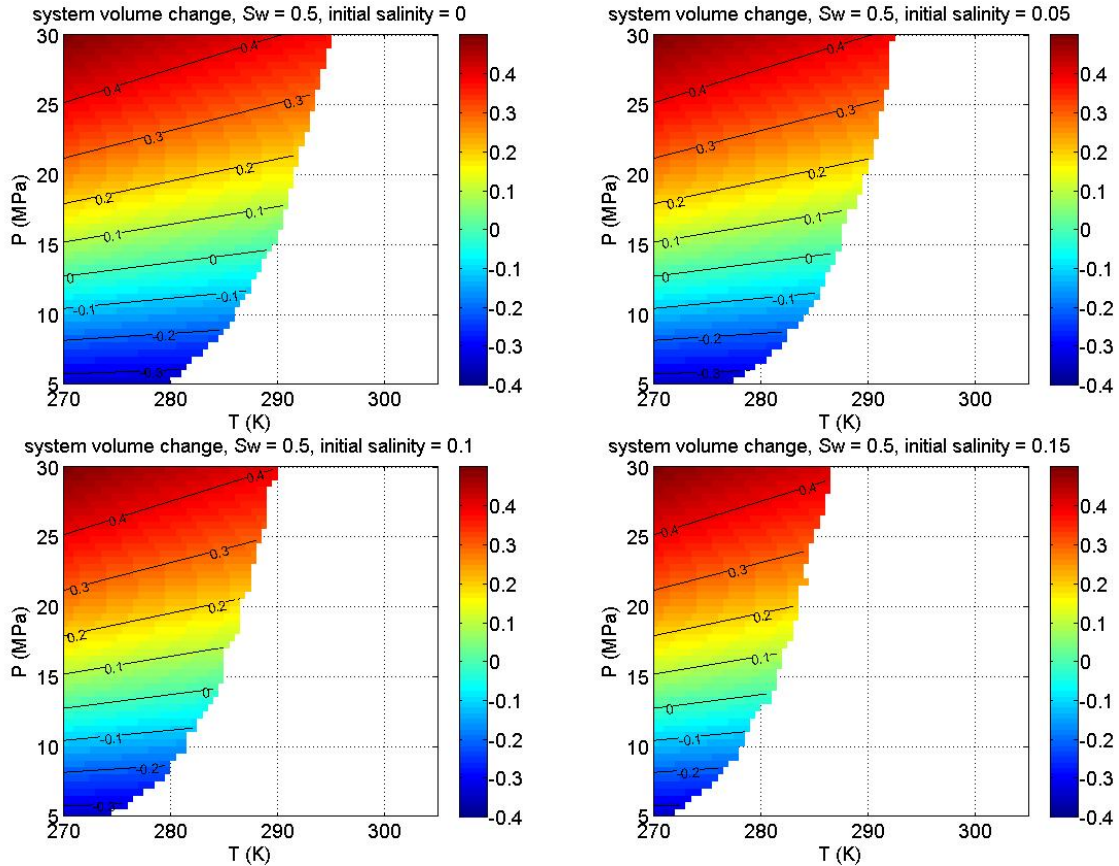
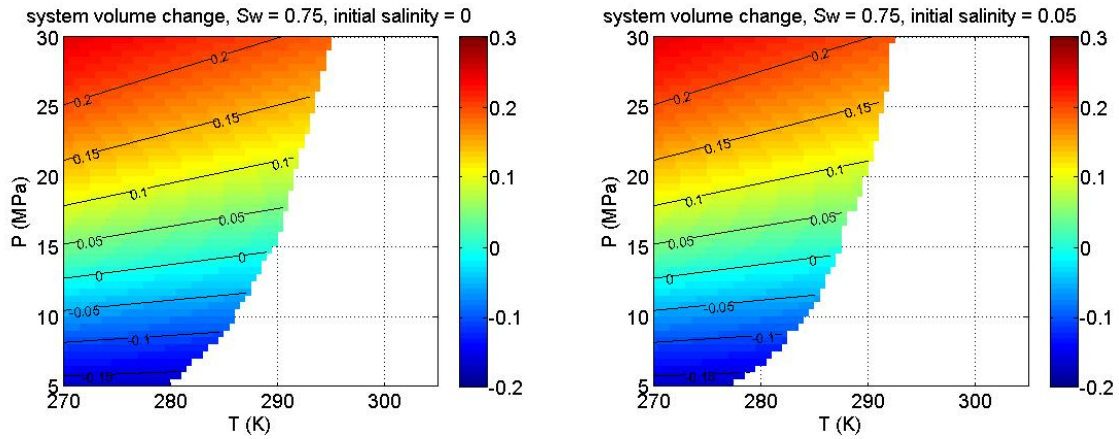


Figure 16. System volume change at $S_w = 0.5$, at four salinities. Since water is unlimited, water saturation is constant. There is no supply of methane from outside the system.



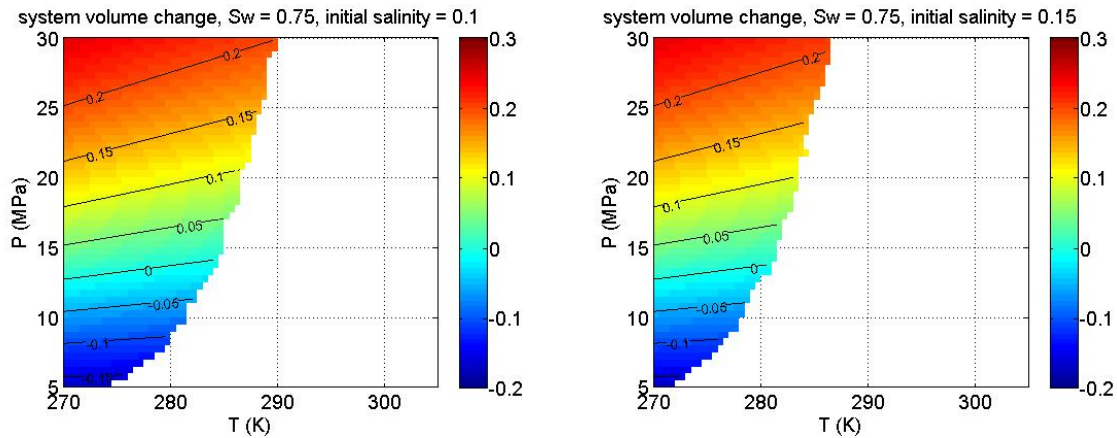


Figure 17. System volume change at $S_w = 0.75$, at four salinities. Since water is unlimited, water saturation is constant. There is no supply of methane from outside the system.

The comparison among Figure 15, 16 and 17 shows that the possible volume change (the absolute value) at a specific T and P decreases as S_w increases. Since the brine volume is constant, the volume change of the system is totally determined by the difference between methane volume and hydrate volume. When S_g , which is $1 - S_w$, decreases, less hydrate can be generated, so that the difference between the volume of methane converted and volume of hydrate generated is reduced, and hence the volume change.

DISCUSSION

Although the scenarios proposed in this section are different – hydrate formation from limited brine and methane vs. hydrate formation from limited methane but unlimited brine – we reach a similar conclusion regarding the effect of initial saturations of gas and brine phases. For both models, lower initial brine saturation S_w leads to the greater volume change. Consequently the greatest need for accommodation, whether by grain movement or by fluid displacement, occurs at small S_w . This corresponds to the situation of hydrate formation after gas has invaded a sediment and displaced brine down to the drainage endpoint.

An important qualitative difference also emerges from the models. In the limited brine and methane scenario, the volume change is always negative, whereas in the limited methane and unlimited brine scenario, the volume change can be negative or positive, depending on the methane density and hence upon T and P .

Under the assumption of the limited brine and methane model, sediment compaction must take place to accommodate the volume change. If mechanical constraints prevent such compaction, *e.g.* if the sediment has already been deeply buried, then the fluid phase pressures will decrease. This will stop hydrate formation when the phase stability boundary is reached. Alternatively, the pressure changes will cause important changes in the grain-scale configuration of the fluids. These effects are considered in the microscale modeling section of this report.

Under the assumptions of the limited methane/unlimited brine model, the negative volume change that occurs at lower values of T and P would require sediment

compaction. If this cannot occur because of mechanical constraints, the gas phase pressure would decrease. The water phase pressure would remain constant because of the presumed connection to bulk aqueous phase. This leads to the same grain-scale reconfiguration problem analyzed in the microscale modeling section of this report.

On the other hand, the positive volume change that occurs at larger values of P would require the sediment to expand. This could induce fractures, whose onset in the gas/water system we have described in previous reports in this project. The onset of fractures in the gas/water/hydrate system can be treated with the same model, subject to suitable assumptions about the mechanical strength of the hydrate, and is the subject of future work in this project. If grain displacement is prevented by the stresses on the sediment and the strength of the gas/water/hydrate/sediment system, then the gas phase pressure would increase. This would rupture the hydrate film, as examined in the microscale modeling section, but would lead subsequently to drainage. This situation will be the subject of future investigation in this project.

References

- Hong, D.N, Gruy, F. and Herri, J., 2006, Experimental data and approximate estimation for dissociation time of hydrate plugs. *Chemical Engineering Science*. 61: 1846-1853
- Uchida, T., Ebinuma, T. and Ishizaki, T., 1999, Dissociation condition measurements of methane hydrate confined small pores of porous glass. *Journal of Physics Chemistry*. 103: 3659-3662

Part 2: Microscale modeling of CH₄-H₂O-Hydrate system

1. Conceptual model

We present here a model which couples multiphase flow, mechanical deformation and hydrate formation in marine sediment. The model extends our previous work, which focused on simulating flow and mechanics, by accounting for the growth of solid hydrate in the sediment pore space. Our model accounts for the distribution of the different methane phases at the grain-scale and its consequences on the sediment dynamics. Such information at the grain-scale, which complements the macroscopic description presented in Part 1 of this report, is crucial to understand phenomena like fracturing and venting. To simulate hydrate growth, we adopt the following assumptions: (1) The timescale associated with nucleation of hydrate crystals and further growth is much larger than that involved in adjustments of the gas-water interface (GWI); (2) Hydrates first form as a thin film along the GWI; (3) Hydrate grow mostly into the water phase; and (4) The hydrate film ruptures if the difference between the gas and water pressure drops below a critical value.

The first assumption allows us to consider hydrate to form given a static sediment configuration; that is, we simulate growth along a static GWI and with no grain rearrangements. Given the episodic nature of the gas recharge in many geological systems [Haeckel *et al.*, 2004; Hester and Brewer, 2009], we consider the following scenario: gas pressure in an external reservoir increases abruptly and allows gas to invade into an initially water-saturated sediment, found within the hydrate stability zone (HSZ). This drainage endpoint provides the starting configuration for simulating hydrate growth. The current model describes the sediment dynamics, including hydrate growth and the related meniscus readjustments, prior to an additional gas recharge event. Thus, the results represent an intermediate stage associated with timescales shorter than those of geologic events such as sedimentation and tectonics. Evaluation of the hydrate saturation at geologic timescales is beyond the scope of this work.

Assumptions 2-3 are used to estimate the hydrate volume and its distribution within the pore space. The extremely low concentrations of both methane in liquid water (about 1000 times lower than in hydrates) and water vapor in methane, together with the high Gibbs free energy associated with the GWI, explain why methane-hydrate nucleation and growth occur at the GWI [Ribeiro and Lage, 2008; Sum *et al.*, 2009]. Recent experiments show that methane-hydrate first form as a thin layer that spreads across the GWI, which then thickens by growing into the water side of the interface [Taylor *et al.*, 2007]. Along with its thickness, the density of the hydrate film increases with time, reducing its transmissibility and thus its growth rate.

In our model, a thin hydrate film grows in all gas pores which are connected to water pores. The film, initially connected throughout the sediment, passes close to the pore throats within these drained pores, and coats parts of the grains which form these pores, see Figure 18. The numerical sample used in our model is a three-dimensional (3D)

packing of spherical grains, allowing account of the complex topology of the GWI which cannot be realized with a two-dimensional (2D) model. Since mass transfer limitations across the porous hydrate film are considered to dominate the film growth rate [Sum *et al.*, 2009], we exclude the effect of heat transfer in our model. Given the low hydrate saturations formed within the short time frame considered here, we also exclude the effect of the related salinity variations.

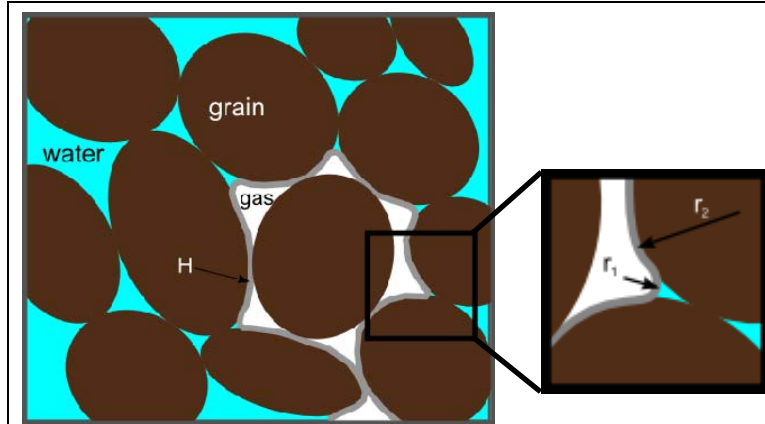


Figure 18: Two-dimensional schematic picture of a hydrate film (in grey) formed at the gas-water interface. The inset shows the radius of curvature of two types of surfaces: (1) at the pore throats, r_1 ; and (2) coating the sediment grains, r_2 . The 3D numerical sample used in our model allows account of the complex hydrate film topology, e.g. connectivity around grain contacts.

Crucial in our model is the account of mechanical instability of the hydrate shell that forms around a gas body. Cracking of a hydrate shell growing around a methane bubble immersed in water was observed in an experiment by Sun *et al.* [2007]. We hypothesize that a similar failure occurs in the weakest parts of a hydrate film within sediments. In a finite body of gas which is not recharged by an external source, the instability arises because of the gas pressure drop associated with the consumption of methane as it is converted to hydrate, see Figure 19.

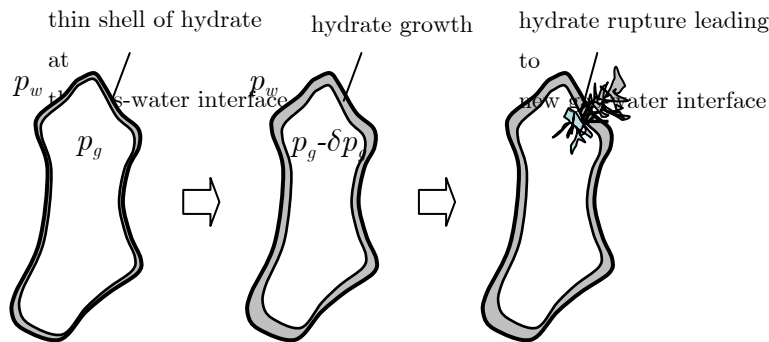


Figure 19: Hydrate precipitates as a thin layer around the gas-water interface. The volume occupied by hydrate is less than that of its stoichiometric components. Thus if the hydrate layer is rigid, the pressure inside the volume of gas will decrease, eventually leading to mechanical instability and rupture of the hydrate shell. This is a potential mechanism for enhancing the mobility of methane gas and providing additional gas-water interface area.

We note that some of the methane that diffuses across the hydrate film may dissolve in the water without increasing the width of the hydrate film; in our model, we neglect variations in dissolved methane saturations and assume that all the gas which diffuses through the hydrate film is consumed by further hydrate formation. We will relax this assumption – and model hydrate dissolution in water – at a later stage.

Upon rupture of the hydrate film, direct gas-water contact is regained and water may imbibe into the drained pores. We simulate imbibition through the ruptured hydrate film, accounting for its arrest due to increase in gas pressure as the volume occupied by a fixed number of methane moles shrinks.

2. Simulation of hydrate growth and gas-water meniscus readjustments

To simulate the initial stages of hydrate growth, including the gas pressure drop and the stability of the hydrate film, one must evaluate the distribution of methane among the different phases, i.e. the number of moles and volume of methane in the gas and hydrate phases. To do so, we make several simplifying assumptions regarding the geometry and topology of the hydrate film.

2.1 Rate of hydrate film thickening and the associated timescales

The increasing thickness and density of the hydrate film reduce the rates in which methane diffuses across the film, making the growth rate highly nonlinear [Taylor *et al.*, 2007]. In our simulations, we increase the film thickness by uniform increments. Thus, the timescales associated with incrementing the film by a unit thickness at later stages are much larger than those at the beginning of the process. To represent the mass-transfer limitations, we assume the growth rate becomes negligible in pores in which the film thickness becomes greater than a certain threshold (e.g. $\frac{1}{2}$ of the pore radii). We note that, while growth rates in these pores may be negligible within the short time frame of our current model, significant growth can occur over longer time periods.

2.2 Hydrate volume

Assuming a thin film, we compute the methane volume, V_H , as the product of the GWI area, A_{GWI} , and the film thickness, ξ . The total interfacial area A_{GWI} is evaluated by summing over the area of individual surfaces from which the GWI is made. Each such surface is associated with a pore on the gas side of the GWI, and includes two pieces: a film across the pore throat (type 1), and a film coating parts of the grains that define that throat (type 2); cf. Figure 18. In our model, each pore is defined by 4 grains, where each throat is associated with 3 grains. Using analogy with hexagonal packing of spheres, the area of each surface is the sum of a type 1 film and 3 parts of grain coating (type 2), where each part makes for $1/6$ of the coating of a single grain. The area of each film type is approximated by assuming that it has the shape of a hemispherical cap, making the area of each surface equal to $2\pi r_1^2 + \pi r_2^2$, where r_1 and r_2 are the radii of the caps near a throat and coating the grains, respectively. Here, $r_1 = (r_{th} + r_p)/2$, r_2 is the arithmetic average of

the grain radii, r_{th} is the Haines insphere radius of the throat and r_p is the effective radius of the gas pore, evaluated by $r_p = (4/3\pi V_p)^{1/3}$ where V_p is the pore volume.

2.3 Gas pressure reduction due to hydrate growth

The reduction in gas pressure due to increase in methane consumption to form hydrate is evaluated using the ideal gas law, $p_g V_g = n_g RT$, where p_g and V_g are the gas pressure and volume, n_g is the number of methane moles, T is the sediment temperature (assumed uniform), and $R=8.314\text{J}/(\text{K mol})$ is the gas constant. Improving the model accuracy by using nonlinear equation of state (EOS), e.g. see Part 1 of this report, is straightforward. Following each incremental change in film thickness, $d\xi$, the associated pressure increment is computed by $dp_g = dn_g RT/V_g$. Since growth occurs into the water phase, V_g remains fixed and the pressure changes linearly with the number of moles. Assuming perfect conversion of gaseous methane to hydrate, i.e. complete filling of the hydrate cages with methane and negligible methane dissolution in water, $dn_g = -dn_H$, where $dn_H = \rho_H V_H / M_H$ is the number of hydrate moles formed at that incremental growth event. Here, ρ_H , V_H , and M_H are the hydrate density, volume, and molar mass, respectively. These assumptions could be relaxed by replacing the 1:1 ratio with $dn_H = -\omega dn_g$, where the value of ω denotes the overall efficiency of methane to hydrate conversion.

2.4 Rupture of hydrate film

Following the experimental observations of wilting and cracking of a hydrate shell growing around methane bubble [Sun *et al.*, 2007], we assume that portions of the hydrate film along the GWI which reside in the pore throats may fail in a similar fashion. The mechanical stability of the films is evaluated using a linear buckling analysis for a spherical cap [Zoelly, 1915]. Assuming each hydrate film within a throat is made of isotropic, homogenous, linearly elastic material, the critical buckling pressure is $p_{cr} = [2E_H(\xi/r_1)^2]/[3(1-\nu_H^2)]^{(1/2)}$, where E_H and ν_H are Young modulus and Poisson ratio of the hydrate film. Thus, a film of curvature $1/r_1$ will fail if $p_w - p_g > p_{cr}$, where p_w is the water pressure. Assuming uniform hydrates stiffness in all pores, the film will rupture first in the pore which has the smallest thickness to radius ratio, ξ/r_1 .

2.5 Imbibition following film rupture

We simulate imbibition through the ruptured film, accounting for the increase in gas pressure: following the imbibition of each pore we determine if p_g suffices to halt imbibition. The pressure following imbibition is computed according to the ideal gas law: $p_g = p_{g,0} V_{g,0} / V_g$, where subscript 0 denotes the value prior to imbibition of the current pore. We assume that the rate of water diffusing through *intact* portions of the hydrate film is negligible relative to that through the ruptured portion, and consider imbibition only at locations in which *direct* gas-water contact is regained. Considering the short timescale associated with GWI readjustments relative to that of hydrate growth, growth is not simulated during imbibition. The computational procedure is outlined below.

Since, by definition, $p_w > p_g$ at failure, the pore on the gas side of the ruptured throat is always imbibed. If p_g allows further imbibition, the order in which additional pores will be imbibed is determined according to their radius – the drained pore of maximum radius among all candidates is selected. The list of candidates for imbibition initially includes only the gas pore connected to the ruptured film. As imbibition continues, additional drained pores which become in direct contact with water are added to the list.

2.6 Further hydrate growth following film rupture and imbibition

Prior to an imbibition event, the hydrate film is contiguous, and its thickness is assumed uniform. We note that if capillary inhibition is important, it may lead to faster growth in larger pores [Clennell *et al.*, 1999]. Since we use numerical samples with a relatively narrow grain-size distribution, we neglect such effect. Following an imbibition event, a new hydrate film will grow along the freshly-exposed GWI, and growth rates at different portions of the sediment will differ. Our preliminary results show that film rupture and imbibition either occurs immediately after the film growth begins, i.e. while the film is extremely thin, or do not occur at all. Therefore, we assume a uniform growth rate in all pores.

Once p_g is sufficiently large to halt imbibition, another growth cycle is simulated in all “active” parts of the hydrate film. Parts of the hydrate film within pores that has been imbibed, as well as those previously ruptured, are considered “inactive”. This distinction is related to the methane availability - inactive portions are no longer in direct contact with gas. For the same reason, inactive portions are not considered as candidates for rupture. While these inactive portions may not play an important role in the short-term hydrate growth, they may contribute to the long-term hydrate distribution, e.g. as nucleation points for hydrate growth following gas recharge and meniscus rearrangements. Growth-imbibition cycles are simulated until growth stops due to mass transfer limitations (see Section 2.1).

2.7 Effect of salinity

Hydrate formation excludes salt and temporarily increases the salinity of the remaining liquid water [Haeckel *et al.*, 2004; Hester and Brewer, 2009]. We compute the salinity increase during the hydrate film growth, and evaluate the associated depression in hydrate equilibrium temperature, ΔT_{eq} . As a first approximation, we estimate ΔT_{eq} from the following empiric relation: $\Delta T_{eq} = -30m_{cl}/m_{sol}$, where m_{cl} and m_{sol} denote the mass of the salt (only chlorine is considered here) and the solution, respectively [Garg *et al.*, 2008]. The reduction in equilibrium temperature T_{eq} reduces the rate of growth, and possibly prohibits growth if T_{eq} falls below the sediment temperature. Note that the local sediment temperature will also rise temporarily due to the latent heat of the exothermic formation process. However, since the coefficient of heat diffusion is much smaller than that of salt, it is reasonable to neglect the effect of latent heat [Clennell *et al.*, 1999].

2.8. Impact of hydrates on the mechanical properties

Hydrate crystals formed at the GWI are expected to act as cement between the sediment grains, due to the presence of residual water around the contacts as pendular rings or capillary bridges. Significant increase in seismic velocities following formation of hydrate at low saturations of 3-5% implies that, in samples with high gas saturation, hydrates cement the grains [Priest *et al.*, 2005].

The effect of hydrate forming intergranular cement will be most noticeable in unconsolidated sediments. Experiments show that the addition of small amounts of cement around the grain contacts, even if the cement material is much softer than the grains, results in a significant increase of the bulk stiffness [Bernabe *et al.*, 1992]. In cemented sediments, additional cement will tend to grow into the pore bodies, thus having a smaller effect on the effective sample stiffness [Dvorkin *et al.*, 1999]. However, cement will have a significant effect on the overall stiffness if deposited along a fracture in consolidated sediment.

Here, we focus on the mechanical effect of hydrate in *unconsolidated* sediments. In our model, hydrates are represented by intergranular cement between the grains that define the pore throats in which hydrate grows, see Section 2.2. We employ the parallel-bond cement model [ITASCA, 2008].

3. Simulation results

3.1 Hydrate distribution in the pore space

To demonstrate the effect of the different mechanisms involved in hydrate formation on the sediment dynamics, we compare simulations using two types of sediments: fine- and coarse-grained sediments, denoted hereafter by FGS and CGS respectively. The drainage endpoint at the first percolation threshold for both FGS and CGS *consolidated* sediment samples is shown in Figure 20. The more ramified invasion pattern in CGS increases the relative contact area between gas and water and leads to an initially larger hydrate saturation upon creation of a thin hydrate film. Enhancing the gas-water contact improves the ability of the methane to traverse the porous hydrate film, which can increase both the rate and the short-term hydrate saturations [Wang *et al.*, 2008]. Moreover, the larger area to volume ratio of the gas body in CGS (320 unit surfaces for the sample in Figure 20) promotes the gas pressure drop with film thickening. The rapid pressure drop together with the larger radius of curvature of the hydrate film in CGS lead to multiple imbibition events, regaining direct connectivity of gas and water and forming new hydrate films within the formerly drained region. Eventually, one is left with sediment which contains many interconnected pieces of hydrate films (455 unit surfaces in the CGS).

The situation is completely different in FGS: the initially smaller gas area to volume ratio (182 unit surfaces) leads to slower decrease in gas pressure upon hydrate growth. Furthermore, the smaller radius of curvature inhibit hydrate film rupture, and thus the film will grow in thickness in an increasingly slower rate due the mass transfer limitation. The hydrate film remains stable, protecting the gas blob from being rapidly converted into hydrate.

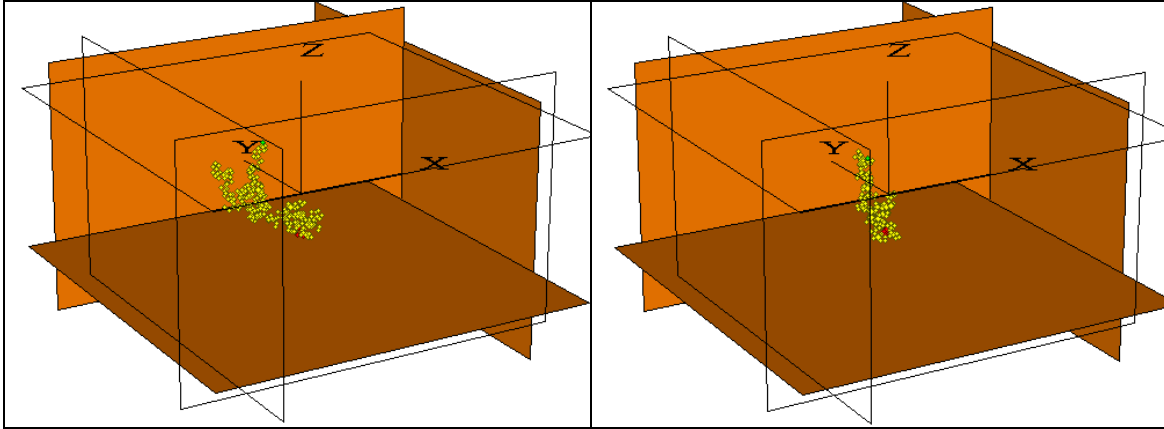


Figure 20: Drainage endpoint at the first percolation threshold for a coarse- (CGS, left) and fine-grained (FGS, right) consolidated sediment. The picture shows the pores invaded by gas as spheres of equivalent volume to that computed from the tessellation. The invasion in the CGS (mean grain diameter of 0.12mm) is characterized by a more ramified pattern and with larger gas saturation (2.5% and 2.2% of pore volume and total number of pores) relative to the FGS (mean grain diameter of 0.12 μ m, saturation of 1.9% and 1.3%, respectively). The difference is due to the preferential flow caused by mechanical deformation in FGS. The deformation in FGS is associated with the larger capillary pressures, $p_c = p_g - p_w$, 2.6MPa, vs. 0.3KPa in CGS.

Another set of simulations was conducted in unconsolidated sediments. The invasion pattern for CGS and FGS is shown in Figure 21. We stress that while the samples used in these simulations lack cohesion related to intergranular cement, meniscus pinning due to surface tension at the GWI near the contacts (in the form of pendular rings or capillary bridges) provides additional source of cohesion. The effect of meniscus pinning on the sediment mechanics and consequently on the flow pattern is significant in unconsolidated FGS, however negligible in CGS or strongly-cemented sediments.

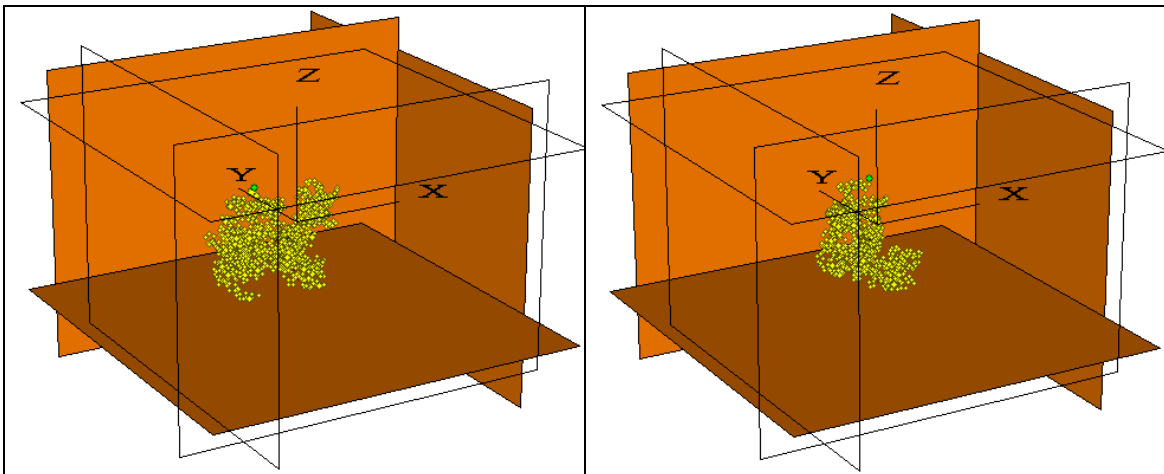


Figure 21: Drainage endpoint at the first percolation threshold for a coarse- (CGS, left) and fine-grained (FGS, right) unconsolidated sediment. The picture shows the pores invaded by gas. The invasion pattern in the CGS (mean grain diameter of 0.1mm) is more ramified, with larger gas saturation (8.7% and 8.2% of pore volume and total number of pores) than the FGS (mean grain diameter of 0.1 μ m, saturation of 5.9% and 5.5%, respectively). Percolation capillary pressures are 4.2MPa and 4.0KPa in the FGS and CGS.

Figure 21 shows that similarly to the simulations with cemented samples, the more ramified invasion pattern together with the lower radius of curvature in CGS leads to failure of the hydrate film and imbibition, whereas in FGS the film remains intact and protects the gas from further conversion into hydrate. Also similar is the short-term hydrate saturation, with imbibition increasing the number of unit surfaces from 969 to 1046 in CGS, vs. only 672 surfaces in FGS. The mechanical effect of hydrate formation, however, is very different than that for consolidated sediments, see Section 3.2.

Finally, we note that in both CGS and FGS, since the hydrate saturations associated with the thin films are extremely small, the effect of salinity is negligible. For instance, for the consolidated samples in Figure 20, the temperature rise is $\sim 0.3^\circ\text{C}$. Thus, unless the sediment is close to the thermodynamic stability limit (e.g. less than 5m above the base of the HSZ for a geothermal gradient of $55^\circ\text{C}/\text{km}$), such depression will have a negligible effect on the formation rate. Similarly, the effect of the latent heat of hydrate formation is expected to be negligible.

3.2 Effect of hydrate formation on the mechanical properties

Here, we demonstrate the impact of hydrate on the mechanical effect of hydrate formation using the unconsolidated samples in Figure 21. In Table 1, we compare the elastic moduli of the CGS and FGS evaluated before and after the hydrate formation, that is without and with intergranular cement in throats where hydrates form. The parallel-bond cement material [ITASCA, 2008] was assigned normal and shear stiffness 10 times smaller than the corresponding average intergranular stiffness values, radius multiplier of 1, and large strength to prohibit breakage. The small perturbations applied in evaluating the moduli justify the latter assumption.

We characterize the mechanical properties through the elastic moduli. The moduli are evaluated by simulating a triaxial test, applying small compressive strain increments (0.01 milistrain) in the axial direction (here y) and zero strain at the lateral direction (x, z). The strains are applied by incremental boundary displacements. The change in stresses, measured from the total forces acting on the boundaries, in response to these perturbations provides the effective moduli using Hooke's law for a homogeneous, isotropic, linearly elastic material [Landau and Lifshitz, 1986]. Two independent moduli, e.g. Young's modulus, E , and Poisson's ratio, ν , are evaluated from Hooke's law. Table 1 also provides additional moduli, computed using the interrelations between the moduli. All moduli in Table 1 are evaluated from the two equations describing Hooke's law in the x and y directions. During the triaxial test simulations we keep the fluid pressures fixed, effectively measuring the *drained* moduli.

In our model, to reduce boundary effects associated with the solid-fluid coupling we separate the solid and fluid domains by defining an inner portion of the granular pack as a "fluid region", while granular mechanics is simulated within the entire pack. Consequently, cementation associated with hydrate formation will be restricted to that region only. Since we evaluate sample-averaged stress and strain values from the forces and displacements at the sample boundaries, the values in Table 1 underestimate the effect of hydrate formation on the mechanical properties. Nonetheless, the results clearly

show that formation of hydrate as intergranular cement will increase the sample stiffness, here by $\sim 10\%$.

Table 1: Elastic moduli of the sediment sample evaluated before and after hydrate formation, which is represented by intergranular cement. E , G , and K are in GPa. Change (in %) is positive for increase.

	E	G	K	ν
CGS - Before	1.51	0.65	0.75	0.16
CGS - After	1.66	0.72	0.82	0.16
CGS – Change	10%	11%	9%	-2%
FGS - Before	1.58	0.67	0.81	0.17
FGS - After	1.78	0.76	0.90	0.17
FGS – Change	13%	13%	12%	-2%

4. Discussion

The conceptual model presented in this work provides a feasible explanation for the strikingly different hydrate distribution and saturation in fine- and coarse-grained marine sediments. Based on experimental observations, we have assumed that hydrate starts forming as a thin film along the GWI, and describe its short-time growth into the adjacent pores. Using a numerical sample in the form of a disordered packing of spherical grains, we determine the location of the hydrate film and quantify the relation between the hydrate volume and the drop in methane pressure. Experiments show that growth is quickly arrested due to mass transfer limitations that evolve as the hydrate film gets thicker and denser. Simple calculations using thermodynamics arguments show that the resulting hydrate saturations are very small, and that methane will remain in its own phase unless another mechanism becomes dominant. We propose that this mechanism is the mechanical rupture of the hydrate film as a result of the drop in gas pressure, and estimate the conditions for rupture using linear elastic buckling analysis. Following rupture of the hydrate film we simulate imbibition into the gas body.

Our simulations show that in CGS, multiple cycles of film growth, rupture and imbibition result in disseminated hydrate distribution, whereas in FGS the film remains stable and the gas will remain in its own phase for longer periods. An experimental investigation to validate our model is underway. These findings may also have important consequences on the long-term hydrate saturations. Since in gas-rich sediment hydrate formation is expected to act as intergranular cement, variations in hydrate saturation and distribution will strongly impact the mechanical properties of the sediment. Finally, we stress that the connectivity of the gas, and consequently its ability to traverse the sediment, are strongly affected by the hydrate distribution. The different storage and transport properties of CGS and FGS are expected to play a significant role in the global carbon cycle.

Bibliography

- Bernabe, Y., Fryer, D.T., and Hayes, J.A. (1992). The effect of cement on the strength of granular rocks, *Geophys. Res. Lett.* 19(14):1511–1514.
- Clennell, M. B., Hovland, M., Booth, J. S., Henry, P., and Winters, W. J. (1999). Formation of natural gas hydrates in marine sediments: 1. Conceptual model of gas hydrate growth conditioned by host sediment properties. *J. Geophys. Res.*, 104(B10):22985–23003.
- Dvorkin, J., Berryman, J. , and Nur, A. (1999). Elastic moduli of cemented sphere packs, *Mechanics of Materials*, 31(7):461–469.
- Garg, S. K., Pritchett, J.W., Katoh, A., Baba, K., and T. Fujii (2008). A mathematical model for the formation and dissociation of methane hydrates in the marine environment, *J. Geophys. Res.*, 113(B01201).
- Haackel, M., Suess, E., Wallmann, K., Rickert, D. (2004). Rising methane gas bubbles form massive hydrate layers at the seafloor. *Geochim. Cosmochim. Acta*, 68(21):4335–4345.
- Hester, K.C. and Brewer P.G. (2009). Clathrate Hydrates in Nature. *Annu. Rev. Marine. Sci.*, 1:303-327.
- ITASCA (2008). PFC3D v4.0, Itasca Consulting Group, Inc., Minneapolis, MN.
- Landau, L.D. and Lifshitz, E.M. (1986). *Theory of Elasticity. Course of Theoretical Physics, Vol 7.* Burlington, MA: Elsevier.
- Vol 7. Burlington, MA: Elsevier. Priest, J.A., Best, A.I. and Clayton, C.R.I. (2005), A laboratory investigation into the seismic velocities of methane gas hydrate-bearing sand, *J. Geophys. Res.*, 110(B04102).
- Ribeiro, C.P. and Lage, P.L.C. (2008). Modelling of hydrate formation kinetics: state-of-the-art and future directions. *Chem. Eng. Sci.* 63:2007–2034.
- Sum, A.K., Koh, C.A., and Sloan E.D. (2009). Clathrate Hydrates: From Laboratory Science to Engineering Practice. *Ind. Eng. Chem. Res.* 48:7457–7465.
- Sun, C.Y., Chen, G.J., Ma, C.F., Huang, Q. Luo, H. and Li, Q.P. (2007). The growth kinetics of hydrate film on the surface of gas bubble suspended in water or aqueous surfactant solution. *J. Crystal Growth* 306:491–499.
- Taylor, C.J., Miller, K.T., Koh, C.A., and Sloan, E.D. (2007). Macroscopic investigation of hydrate film growth at the hydrocarbon/water interface. *Chem. Eng. Sci.*, 62: 6524–6533.
- Wang, W., Bray. C.L., Adams, D.J., and Cooper, A.I. (2008). Methane storage in dry water gas hydrates. *J. Am. Chem. Soc.*, 130(35):11608–11609.
- Zoelly R. *Über ein Knickungsproblem an die Kugelschale.* PhD Dissertation, TH Zurich, 1915.

National Energy Technology Laboratory

626 Cochrans Mill Road
P.O. Box 10940
Pittsburgh, PA 15236-0940

3610 Collins Ferry Road
P.O. Box 880
Morgantown, WV 26507-0880

One West Third Street, Suite 1400
Tulsa, OK 74103-3519

1450 Queen Avenue SW
Albany, OR 97321-2198

2175 University Ave. South
Suite 201
Fairbanks, AK 99709

Visit the NETL website at:
www.netl.doe.gov

Customer Service:
1-800-553-7681

